

Technische Universität Wien

Diplomarbeit

On-chip microfluidic cell separator based on dielectrophoresis

Ausgeführt zum Zwecke der Erlangung des akademischen Grades eines Diplom-Ingenieurs
unter der Leitung von

Univ. Prof. Dr. Michiel J. Vellekoop

und

Dipl.-Ing. Stefan Kostner

Institut für Sensor- & Aktuatorssysteme

eingereicht an der Technischen Universität Wien
Fakultät für Elektrotechnik und Informationstechnik

von

Jürgen Avian

Matr.Nr.: 9925384

Pelzgasse 12/21, 1150 Wien

Wien, im Juni 2007

Abstract

In this work a microfluidic device for the continuous separation of particles with a diameter of a few micrometers, like biological cells, was developed. The separation is based on dielectrophoresis which is a common method for particle manipulation in microfluidic systems. In contrast to existing separator devices which mainly rely on negative dielectrophoresis the design presented in this work utilizes both, positive and negative dielectrophoresis.

The particles are transported by a fluid flow past the platinum electrodes placed at the bottom of the channel. These electrodes produce the inhomogeneous electric field needed for the dielectrophoretic effect that deflects the particles on their path through the separation channel. Prior to the actual separation process hydrodynamic focusing of the particles into the center of the channel takes place to ensure a common starting position.

The correct function of the device was proved and evaluated by separation experiments with yeast cells ($d \sim 5 \mu m$) and polystyrene beads ($d = 8 \mu m$). At a voltage of $11.3 V_{RMS}$ and a frequency of $1 kHz$ the yeast cells and beads showed positive and negative dielectrophoretic behavior, respectively.

Kurzfassung

Es wurde ein Biochip zur kontinuierlichen Separation von Partikeln mit einer Größe von einigen Mikrometern, wie etwa biologische Zellen, entwickelt. Die Separation basiert auf dem physikalischen Effekt der Dielektrophorese die im Bereich der Partikelmanipulation mittels mikrofluidischen Systemen weite Anwendung findet. Im Gegensatz zu den vorhandenen Systemen die vorwiegend auf negativer Dielektrophorese basieren kann mit dem vorliegenden Chip sowohl positive als auch negative Dielektrophorese genutzt werden.

Die Partikel werden in einer Flüssigkeitsströmung durch den Kanal an Platin-Elektroden vorbei transportiert. Diese Elektroden erzeugen das für die Dielektrophorese notwendige inhomogene elektrische Feld wodurch die Partikel auf ihrem Weg durch den Separationskanal horizontal abgelenkt werden. Vor dem eigentlichen Separationsprozess wird eine hydrodynamische Fokussierung der Partikel in die Mitte des Kanals durchgeführt um eine einheitliche Startposition zu gewährleisten.

Die Funktion des Chips wurde durch Separationsexperimente mit Hefezellen ($d \sim 5 \mu m$) und Polystyrol-Partikel ($d = 8 \mu m$) bestätigt und evaluiert. Bei einer angelegten Spannung von $11.3 V_{RMS}$ und einer Frequenz von $1 kHz$ zeigen Hefezellen positive und Polystyrol-Partikel negative Dielektrophorese.

Acknowledgments

First I want to thank Univ. Prof. Dr. Michiel J. Vellekoop for the possibility to work in such an interesting and evolving field of research and for his support throughout this work. Without the personal commitment and the technical advice of my mentor Dipl.-Ing. Stefan Kostner even on weekends this research project would not have been such a success.

Many thanks to my colleagues at the *Institute of Sensor and Actuator Systems* for their technological advice regarding the device fabrication and its realization (in alphabetical order): Dr. Artur Jachimowicz, Ing. Edeltraud Svasek, and Ing. Peter Svasek.

Furthermore many thanks to Dipl.-Ing. Markus Luchner, *University of Natural Resources and Applied Life Sciences, Vienna*, for his advice regarding biological materials and know-how.

Special thanks to the woman of my life who supported me and backed me up mentally especially during the last few weeks before the finalization of the project.

Many thanks to my parents who shaped me and supported me financially in the last years.

Contents

1	Introduction	1
2	Theory	3
2.1	Introduction	3
2.2	Dielectrophoretic force	3
2.2.1	Lossless sphere in dielectric medium	4
2.2.2	Dielectric particles with ohmic loss	5
2.2.3	Layered dielectric particles with ohmic loss	6
2.3	Drag force	8
2.4	Buoyancy and gravity force	8
2.5	Theoretical model of particle movement	9
3	Simulation	11
3.1	Introduction	11
3.2	Estimation of Clausius Mossotti factor for yeast and E. coli	11
3.3	Electric field simulation	14
3.4	Fluid flow simulation	16
3.5	Simplifications for the simulation	18
3.6	Optimization of electrode geometry in 2D	19
3.6.1	Plotting trajectories for optimized design geometry	25
3.7	Verification of the simulation results in 3D	26
4	Device	28
4.1	Introduction	28
4.2	Practical considerations	28
4.2.1	Particle sedimentation	28
4.2.2	Joule heating	30
4.2.3	Electrode erosion	34
4.2.4	Suspension properties	35
4.3	Concept	36
4.3.1	Sample injection and particle focusing	36
4.3.2	Particle separation	38
4.3.3	Evaluation of separation process and sample outlet	40
4.4	Design considerations	40
4.4.1	Requirements	41
4.4.2	Channel dimensions of the design variations	41
4.5	Materials and fabrication process	42

5	Measurements	46
5.1	Experimental setup	46
5.1.1	Device holder	47
5.1.2	Voltage supply	48
5.1.3	Printed circuit board for device bonding	48
5.2	Measurement work flow	49
5.2.1	Detection of the particle position	50
5.3	Measurement results	51
5.4	Interpretation	52
6	Discussion	55
6.1	Separation efficiency	56
6.2	Device improvements	57
6.3	Outlook	57
A	Model implementation in Matlab	60
B	Device fabrication masks	69
C	Measurement work flow	73
D	μTAS 2007 conference abstract	75

1 Introduction

In this work a new concept for continuous separation of small particles in a microfluidic device based on dielectrophoresis was developed. To prove the theoretical results a microfluidic device was fabricated to test the separation efficiency with samples containing polystyrene beads and biological cells of different size and electrical properties.

To get an idea of the principle of the device presented in this work the schematic function of the separation process is shown in figure 1.1 as a view on top of the device.

In section (A) the beads or cells are injected through the sample inlet etched into the bottom of the device. The sheath flow moves the sample to the taper where the particles are pre-focused horizontally. In section (B) the second focusing via the sideport flow aligns the particles in a confined row so that all of them enter the separation zone at the same horizontal position. In the separation zone in section (C) the aligned particles are separated due to their differing size and electrical properties that cause a different dielectrophoretic (DEP) force acting on them. The DEP force is produced by plane electrodes placed at the bottom of the channel which create the necessary inhomogeneous electrical field.

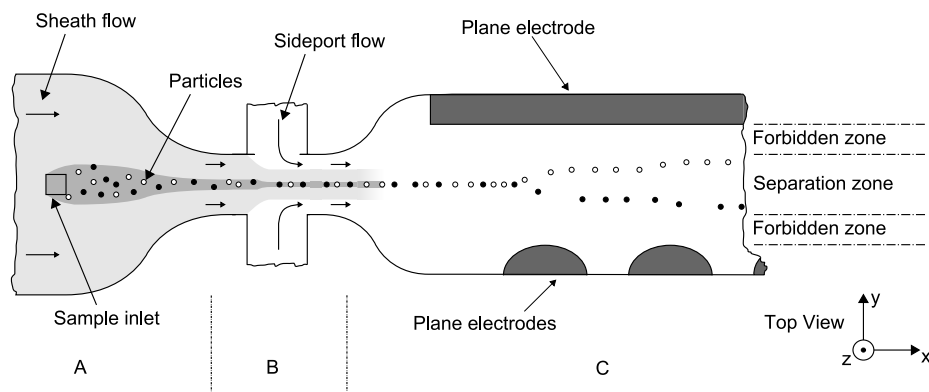


Figure 1.1: Schematic of the separation process. After injection of the particles (A) and focusing (B) they are separated due to their size and electrical properties by the dielectrophoretic force acting on them (C).

The separation zone was chosen such that the particles do not enter areas where the DEP force shows extreme values and the chance of trapping is high (forbidden zones). That may occur especially at the electrode edges. Depending on electrical properties of the particles they are either moved towards the round electrodes (black particles, positive DEP) or away from them (white particles, negative DEP).

Chapter 2 explains the theory for the forces that were taken into account in the model and tries to estimate the dielectrophoretic behaviour of biological cells.

Chapter 3 covers the simulation of the model and presents the optimized electrode geometries for an efficient separation of particles passing the separation zone.

In chapter 4 both the design requirements for the device and the fabrication process are covered that lead to the final device.

The experimental setup and the results of the separation measurements are summarized in chapter 5 and the agreement of this results with the device simulation is evaluated. That leads to possible improvements of the design that are outlined in chapter 6.

2 Theory

2.1 Introduction

In this chapter the theoretical background for the separation process is introduced and a model for the ensuing simulation is developed. The final model accords to that found in [Kostner, 2004] where it is described in depth. Therefore the explanations in this chapter are kept short in order to explain the simulation tasks in detail in the next chapter.

To separate particles in terms of size and electrical characteristics a force called the dielectrophoretic force is utilized that depends on those properties. The theory of the dielectrophoretic effect is described by Jones [Jones, 1995] in detail.

To achieve a continuous separation the particles are moved along the separation channel in a hydrodynamic flow that applies a drag force. The DEP force acts perpendicular to the flow direction.

The function of the device presented in this work is based solely on those two types of forces. Beside them other forces like the buoyancy and gravity force have to be taken into account and are discussed in section 2.4.

Since these forces act independently from each other they can first be calculated on their own and then be combined to a complete model for the force acting on the particles as shown in section 2.5.

The last section of this chapter is an attempt to predict the expected behaviour of yeast cells and *E. coli* bacteria in a dielectrophoretic force field and it is based on the electrical properties of those model organisms.

2.2 Dielectrophoretic force

The dielectrophoretic force acts on polarizable objects in an inhomogeneous electric field. In figure 2.1 the principle of the dielectrophoretic effect is shown.

First we consider a dipole in an electric field. Because of the inhomogeneous electric field the *Coulomb Force* acting on these separated charges differs both in value and direction and results in a net force, given in the following equation

$$\mathbf{F}_{net} = q\mathbf{E}(\mathbf{r} + \mathbf{d}) - q\mathbf{E}(\mathbf{r}) \quad (2.1)$$

where \mathbf{F}_{net} is the net force, q is the absolute value of the charges of the dipole and $\mathbf{E}(\mathbf{r} + \mathbf{d})$ and $\mathbf{E}(\mathbf{r})$ are the electric field forces at the locations \mathbf{r} and $\mathbf{r} + \mathbf{d}$, respectively.

A vector Taylor series expansion and elimination of all terms of higher order gives:

$$\mathbf{F}_{dipole} = \mathbf{p} \cdot \nabla \mathbf{E} \quad \text{with} \quad \mathbf{p} = q\mathbf{d} \quad (2.2)$$

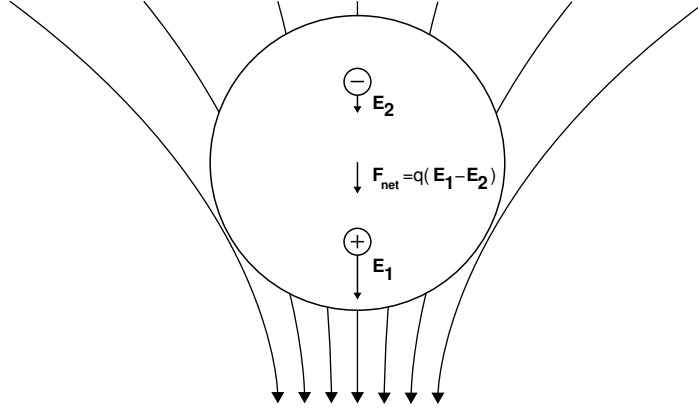


Figure 2.1: Principle of the dielectrophoretic force. The particle is polarized into positive and negative charges which experience different dielectrophoretic forces caused by the inhomogeneous electric field resulting in a net force F_{net} .

where \mathbf{F}_{dipole} is the force acting on the dipole with a dipole moment \mathbf{p} that depends on the gradient of the electric field force $\nabla\mathbf{E}$.

An uncharged, non-polarized particle would not experience any force even in an inhomogeneous electric field since its dipole moment $\mathbf{p} = 0$. But if positive and negative charges in a polarizable particle are separated due to the imposed electric field it appears as a dipole and the dielectrophoretic force takes effect. To calculate the moment of such a particle the effective moment method is used [Jones, 1995, p. 9].

The effective dipole moment \mathbf{p}_{eff} is defined as the moment of an equivalent, free-charge, point dipole that produces the same dipolar electrostatic potential. It is calculated by comparing the electrostatic potential Φ_{dipole} of a point dipole to the electrostatic potential outside of the particle of interest. The electrostatic potential of a point dipole is

$$\Phi_{dipole} = \frac{\mathbf{p}_{eff} \cos\theta}{4\pi\epsilon_1 r^2} \quad (2.3)$$

where θ and r are the polar angle and radial position in spherical coordinates and ϵ_1 is the permittivity of the dielectric medium.

2.2.1 Lossless sphere in dielectric medium

For a dielectric sphere in a dielectric medium the effective dipole moment is

$$\mathbf{p}_{eff} = 4\pi\epsilon_1 K(\epsilon_2, \epsilon_1) R^3 E_0 \quad \text{with} \quad K = \frac{\epsilon_2 - \epsilon_1}{\epsilon_2 + 2\epsilon_1}. \quad (2.4)$$

where ϵ_2 and ϵ_1 are the permittivities of the suspension medium and the particle, respectively. K is the Clausius Mossotti factor ranging from -0.5 to 1 that only depends on the electrical properties for the fluid and the particle. This equation is the result of the effective moment method using the boundary conditions for calculating the electrostatic potential outside the sphere.

Using (2.4) in (2.2) results in the expression for the dielectrophoretic force acting on a dielectric sphere in a dielectric medium

$$\mathbf{F}_{DEP} = 4\pi\varepsilon_1 K(\varepsilon_2, \varepsilon_1) R^3 \underbrace{E_0 \cdot \nabla E_0}_{\frac{1}{2}E_0^2} \quad (2.5)$$

and in a more simplified form

$$\mathbf{F}_{DEP} = 2\pi\varepsilon_1 K(\varepsilon_2, \varepsilon_1) R^3 \nabla E_0^2. \quad (2.6)$$

If periodic AC signals are used to generate the electric field then E_0 and therefore \mathbf{F}_{DEP} are periodic too. A more convenient form of (2.6) is given by

$$\langle \mathbf{F}_{DEP}(t) \rangle = 2\pi\varepsilon_1 K(\varepsilon_2, \varepsilon_1) R^3 \nabla E_{rms}^2 \quad (2.7)$$

where $\langle \mathbf{F}_{DEP}(t) \rangle$ is the time-average of the dielectrophoretic force and E_{rms} is the root-mean-square magnitude of the imposed AC electric field. That is an important simplification since the dielectrophoretic effects simulated in chapter 3 are based on the time-averaged dielectrophoretic force and can be related to the provided root-mean-square voltage at the electrodes. An additional equation that is used in the optimization task simplifies the calculation of the dielectrophoretic force field if the applied voltage varies:

$$\langle \mathbf{F}_{DEP}(t) \rangle \propto E_{rms}^2 \propto U_{rms}^2. \quad (2.8)$$

2.2.2 Dielectric particles with ohmic loss

Since biological cells are not lossless particles the results of the previous section have to be extended to reflect the electric loss occurring in the cell interior. In [Jones, 1995] it is shown that for particles with loss the scalar permittivities in equation 2.4 have to be replaced by their complex counterparts as in

$$\mathbf{p}_{eff} = 4\pi\varepsilon_1 \underline{K}(\underline{\varepsilon}_2, \underline{\varepsilon}_1) R^3 E_0 \quad \text{with} \quad \underline{K} = \frac{\underline{\varepsilon}_2 - \underline{\varepsilon}_1}{\underline{\varepsilon}_2 + 2\underline{\varepsilon}_1} \quad (2.9)$$

where $\underline{\varepsilon}_x$ are the complex dielectric constants

$$\underline{\varepsilon}_1 = \varepsilon_1 + \frac{\sigma_1}{j\omega} \quad (2.10)$$

$$\underline{\varepsilon}_2 = \varepsilon_2 + \frac{\sigma_2}{j\omega} \quad (2.11)$$

where ε_1 and σ_1 are the dielectric permittivity and the conductivity of the fluid and ε_2 and σ_2 are the corresponding values for the particle. The Clausius Mossotti factor K now depends on the frequency. In [Jones, 1995] it is shown that for the time-averaged dielectrophoretic force only the real part of the complex Clausius Mossotti factor takes effect and that leads to

$$\langle \mathbf{F}_{DEP}(t) \rangle = 2\pi\varepsilon_1 \text{Re}[\underline{K}(\underline{\varepsilon}_2, \underline{\varepsilon}_1)] R^3 \nabla E_{rms}^2. \quad (2.12)$$

2.2.3 Layered dielectric particles with ohmic loss

Biological cells are not homogeneous spheres. They consist of cell wall, membranes, and the cell interior which have different electrical properties. A simple but adequate model for biological organisms is the layered dielectric shell model shown in figure 2.2.

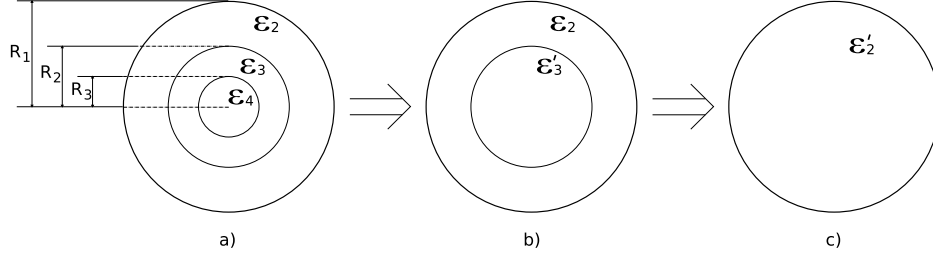


Figure 2.2: Replacement of layered particle with homogeneous sphere. The layers of the particle in a) are successively replaced by equivalent inner spheres with a replacement value for the permittivity. This step is repeated until the original particle is replaced by an equivalent, homogeneous sphere (c).

It consists of several layers with different values for their electrical properties.

To calculate the equivalent dielectric permittivity for a multilayered particle first an equation is derived for a two shell particle that looks like the one in figure 2.2 b) with the dielectric permittivities ε_2 and ε_3 [Jones, 1995, p. 227]. Then the electric potential inside and outside the particle can be written as

$$\phi_1 = \left(-E_0 r + \frac{A}{r^2}\right) \cos\theta, \quad r > R_1 \quad (2.13)$$

$$\phi_2 = \left(-B r + \frac{C}{r^2}\right) \cos\theta, \quad R_1 > r > R_2 \quad (2.14)$$

$$\phi_3 = -D r \cos\theta, \quad r < R_2. \quad (2.15)$$

Applying the boundary conditions at $r = R_1$ and $r = R_2$

$$\phi_1 = \phi_2, \quad \varepsilon_1 \frac{\partial \phi_1}{\partial r} = \varepsilon_2 \frac{\partial \phi_2}{\partial r} \quad \text{at } r = R_1 \quad (2.16)$$

$$\phi_2 = \phi_3, \quad \varepsilon_2 \frac{\partial \phi_2}{\partial r} = \varepsilon_3 \frac{\partial \phi_3}{\partial r} \quad \text{at } r = R_2 \quad (2.17)$$

$$(2.18)$$

and solving the resulting equation system for A gives

$$A = \frac{\varepsilon'_2 - \varepsilon_1}{\varepsilon'_2 + 2\varepsilon_1} R_2^3 E_0 \quad (2.19)$$

with

$$\varepsilon'_x = \varepsilon_x \left\{ \frac{a^3 + 2 \left(\frac{\varepsilon_{x+1} - \varepsilon_x}{\varepsilon_{x+1} + \varepsilon_x} \right)}{a^3 - \left(\frac{\varepsilon_{x+1} - \varepsilon_x}{\varepsilon_{x+1} + \varepsilon_x} \right)} \right\} \quad \text{with} \quad a = \frac{R_x}{R_{x+1}}. \quad (2.20)$$

A multilayered particle will be replaced by a homogeneous particle with the equivalent permittivity ε_2 by applying equation 2.20 successively from inside to outside of the layered sphere. For dielectric spheres with ohmic loss the scalar permittivity ε_x is replaced by the complex permittivity $\underline{\varepsilon}_x$ according to equation 2.11. A further simplification can be derived for particles with thin surface layers if the thickness Δ of the layer is very small compared to the overall radius R of the particle, see figure 2.3. Solving the current continuity conditions and the boundary conditions for the electrostatic potential at $r = R$ gives the same expression for the coefficient \underline{A} as shown in equation 2.19. The mentioned conditions are

$$(j\omega c_m + g_m)(\underline{\phi}_1 - \underline{\phi}_2) = -j\omega \underline{\varepsilon}_1 \underline{E}_{r1} \quad \text{at} \quad r = R \quad (2.21)$$

$$\underline{\varepsilon}_1 \underline{E}_{r1} = \underline{\varepsilon}_2 \underline{E}_{r2} \quad \text{at} \quad r = R \quad (2.22)$$

$$(2.23)$$

where \underline{E}_{r1} and \underline{E}_{r2} are the radial components of the electric field $E_r = -\partial\phi/\partial r$ at the outer and inner side of the particle at $r = R$. The same applies to $\underline{\phi}_1$ and $\underline{\phi}_2$ for the electrostatic potential at the outer and inner side of the thin layer. c_m is the surface capacitance and g_m is the surface transconductance of the thin layer. The expression for $\underline{\varepsilon}'_2$ for thin surface layers is

$$\underline{\varepsilon}'_2 = \frac{c_m R \underline{\varepsilon}_2}{c_m R + \underline{\varepsilon}_2} \quad \text{with} \quad c_m = c_m + \frac{g_m}{j\omega} \quad (2.24)$$

$$c_m = \frac{\varepsilon_m}{\delta} \quad \left[\frac{F}{m^2} \right]$$

$$g_m = \frac{\sigma_m}{\delta} \quad \left[\frac{S}{m^2} \right]$$

With these equations the calculations for the Clausius Mossotti factor for different cell types are performed in section 3.2.

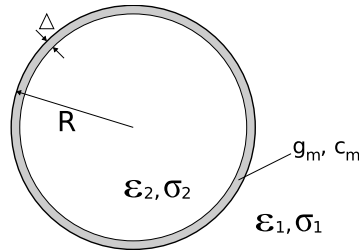


Figure 2.3: Thin surface layer model for the calculation of the equivalent complex permittivity of a thin layered sphere.

2.3 Drag force

The particles are moved inside the device due to microfluidic flow which exerts a drag force on the particles. For the calculation of the drag force a simplification of the Navier Stokes equations is used which is defined for *creeping flow* with a Reynolds Number $Re \ll 1$. That leads to to

$$F_D = 6\pi\eta R(v_f - v_p) = k_1(v_f - v_p) \quad (2.25)$$

where F_D is the drag force, η is the viscosity, R is the particle radius and v_f and v_p are the velocity of the fluid and particle, respectively. Equation 2.25 assumes that the fluid flow is non turbulent which is expressed with a Reynolds Number below unity. For particles of diameters smaller than $5 \mu m$ the Reynolds Number is

$$Re = \frac{\rho v_f L}{\mu} = \frac{1000 \frac{kg}{m^3} \cdot 10^{-3} \frac{m}{s} \cdot 5 \cdot 10^{-6} m}{10^{-3} \frac{kg}{m \cdot s}} = 0.005 \quad (2.26)$$

where ρ is the density of the fluid, L is the particle diameter, and μ is the dynamic viscosity of the fluid.

2.4 Buoyancy and gravity force

On a particle placed in a fluid two additional forces, namely the buoyancy and gravity force, take effect which are oriented anti parallel to each other and can therefore be combined to one resulting scalar force

$$F_B = \rho_f g V_f \quad (2.27)$$

$$F_G = \rho_p g V_p \quad (2.28)$$

$$F_{BG} = F_G - F_B = gV(\rho_p - \rho_f) \quad \text{with} \quad V = V_f = V_p \quad (2.29)$$

where F_B and F_G are the buoyancy and gravity force, respectively, ρ_f and ρ_p are the densities of the fluid and the particle, V_f and V_p are the volumes of the displaced fluid and the particle, and g is the acceleration of gravity. Since the displaced volume of the fluid and the volume of the particle are the same V_f and V_p are replaced by V .

The direction of the buoyancy and gravity force is perpendicular to the dielectrophoretic and drag force due to the separation principle shown in figure 1.1, as long as the device is proper oriented, and therefore these forces do not influence the separation process. Nevertheless it is necessary to estimate the effect of these forces that may occur, for example in form of sedimentation.

An equation for the sedimentation velocity will be derived based on equation 2.25 and 2.29. If the mass density of the particle is greater than that of the fluid, the particle will sediment towards the bottom of the channel and vice versa. It accelerates until the sedimentation

force and the drag force that works against it reach an equilibrium. Then the particle moves with a constant velocity v_p that is derived as follows:

$$\begin{aligned} F_{BG} &= gV(\rho_p - \rho_f) \\ F_D &= 6\pi\eta Rv_p \end{aligned}$$

v_f in equation 2.25 is set to 0 because only the drag of the fluid exerted upon the particle is of interest. In equilibrium F_{BG} and F_D are equal so v_p can be expressed as

$$\begin{aligned} v_p &= \frac{gV(\rho_p - \rho_f)}{6\pi\eta R} \\ &= \frac{g\frac{4}{3}\pi R^3(\rho_p - \rho_f)}{6\pi\eta R} \\ v_p &= \frac{2}{9} \frac{gR^2(\rho_p - \rho_f)}{\eta} \end{aligned} \quad (2.30)$$

where v_p is the sedimentation velocity of the particle. If $\rho_p < \rho_f$ then v_p is negative and the particle moves against the direction of gravity

In section 4.2.1 this equation is used to estimate the influence of the differences of the particle and fluid densities on the particle movement through the separation channel. It will be shown that the particle displacement due to the sedimentation force is negligible.

2.5 Theoretical model of particle movement

The equations derived in the previous sections are combined to a continuous model that describes the particle behaviour and that will be simulated in the next chapter. The buoyancy and gravity force are not taken in account as stated in the previous section. Figure 2.4 illustrates the participating forces.

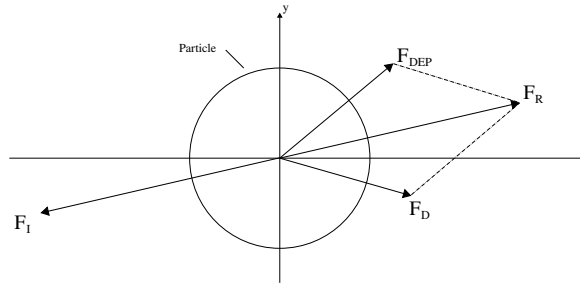


Figure 2.4: Equilibrium of the force F_R , result of the dielectrophoretic force F_{DEP} and the drag force F_D , and the inertia force F_I .

Beside the dielectrophoretic force F_{DEP} and the drag force F_D a third force has to be introduced, the inertia force F_I , that countervails the force F_R which is a result of F_{DEP} and F_D . The equations for this equilibrium can be solved with a linear first order differential equation. All forces can be split in their components in x and y direction and can be independently calculated which results in a simplified scalar equation for each direction. The following equations illustrate the common solution and can therefore considered as the solution for both the x and y direction. The equation for the equilibrium is

$$F_{DEP} + F_D = F_I \quad (2.31)$$

$$F_{DEP} + k_1(v_f - v) = m \frac{dv}{dt} \quad (2.32)$$

$$\frac{dv}{dt} + \frac{k_1}{m}v = \frac{F_{DEP} + k_1v_f}{m} \quad (2.33)$$

where F_D is replaced by equation 2.25 and v_p is replaced by v . This linear differential equation can be solved by multiplying both sides by $e^{\frac{k_1}{m}t}$ which leads to the solution

$$v = \frac{F_{DEP} + k_1v_f}{k_1} + Ce^{-\frac{k_1}{m}t}. \quad (2.34)$$

with the integration constant C that can be calculated applying the initial condition for $t = 0$. Since the inertia force is small compared to the dielectrophoretic force and drag force it can be neglected. The last term in equation 2.34 can be set to 0. The resulting equation can be derived based on $F_{DEP} + k_1(v_f - v) = 0$, too. It is important to note that the dielectrophoretic force is considered to be constant in equation 2.34. To get valid results for the simulation of the particle trajectories it is important that the change of the dielectrophoretic force between two simulation steps is as small as possible, otherwise the solution would be imprecise, see figure 2.5.

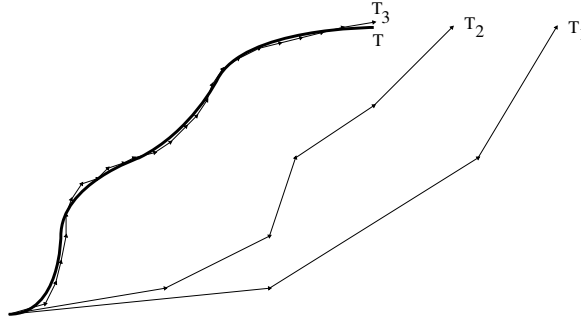


Figure 2.5: Particle trajectories T_x for different calculation time step sizes. For large time steps (T_1 , T_2) the solution differs strongly from the real trajectory (T). Small time steps (T_3) lead to a more accurate result.

3 Simulation

3.1 Introduction

In this chapter the model derived in section 2.5 is simulated and the electrode geometry is optimized using the modeling package COMSOL Multiphysics 3.2b and MATLAB 7.0.4 R14 SP2.

First the Clausius Mossotti factor for different biological cell types is calculated in section 3.2 based on the equations derived in chapter 2 and electrical parameters found in literature. Due to the fact that the electric field and fluid flow are independent from each other their simulation can be performed in separate tasks in the sections 3.3 and 3.4.

Then in section 3.5 possible simplifications for the simulation are discussed.

Since the model simulation can be reduced to two dimensional calculations the complexity of the optimization is significantly decreased. In section 3.6 the geometry of the electrodes and their size and spacing is optimized.

In section 3.7 the optimized model is simulated in a three dimensional setup and validated against the results of the two dimensional simulation.

3.2 Estimation of Clausius Mossotti factor for yeast and E. coli

In this section the dielectrophoretic behavior of yeast and E. coli based on calculations and experiments found in existing literature is analyzed. The results should be a base for decisions regarding the design, like optimization for positive or negative DEP force.

In figure 3.1 the Clausius Mossotti factor is shown as a function of the frequency for different values of the conductivity of the media. The values for the parameters and the used model for the simulation have been taken from the literature ([Jones, 1995], [Zhou et al., 2002], [Suzuki et al., 2005], [Hölzel, 1999], [Hölzel, 1997], and [Hölzel, 2002]).

It is nearly impossible to determine the correct behavior of the two cell types because every source uses another assumption for the model of the cell and its parameters. The used models are two, three, and four shell models with thick layers (layer parameter ε , σ) and thin layers (layer parameter g , c), see section 2.2.3. Additionally the parameters of different cell strains of yeast or E. coli can differ. The conclusion was that the device should not be designed to rely on one type of dielectrophoretic behavior only but rather be able to separate particles with different DEP response as well.

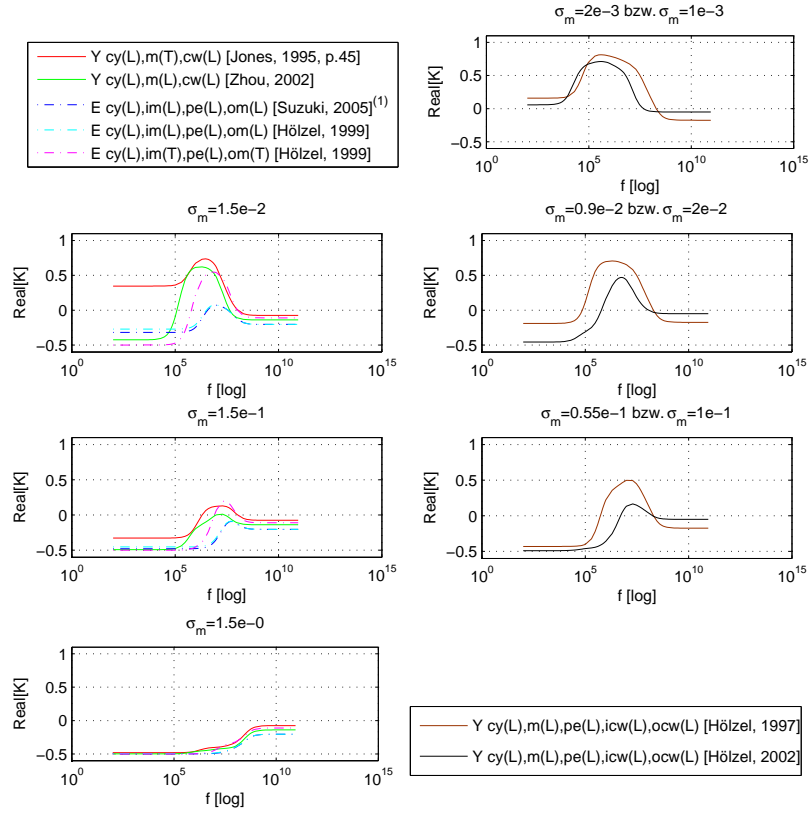


Figure 3.1: Clausius Mossotti factor as a function of the frequency f for various media conductivities and simulation models. In each row the graphs for similar media conductivity is shown. The legend for the left column is in the upper left, the legend for the right column can be found in the lower right corner of the figure. The number of shells used in the model is written in parenthesis. (L) and (T) denote the type of layer model used, (L) means thick layer and (T) stands for thin layer.

Table 3.1 summarizes the model parameters for the Clausius Mossotti factor simulation in figure 3.1.

Reference		Cytoplasm	1 st shell	2 nd shell	3 rd shell	4 th shell
[Jones, 1995, p.45]	r	$2\mu m$		$0.5\mu m$		
	ϵ	60		65		
	σ	$0.5\frac{S}{m}$		$0.1\frac{S}{m}$		
	c		$10\frac{mF}{m^2}$			
	g		0			
[Zhou et al., 2002]	r	$4\mu m$	$8nm$	$0.22\mu m$		
	ϵ	50	6	60		
	σ	$0.2\frac{S}{m}$	$0.25\frac{\mu S}{m}$	$14\frac{mS}{m}$		
[Suzuki et al., 2005]	r	$2\mu m$	$50nm$	$70nm$	$11nm$	
	ϵ	60	3	60	3	
	σ	$0.44\frac{S}{m}$	$0.1\frac{mS}{m}$	$6\frac{mS}{m}$	$2.5\frac{mS}{m}$	
[Hölzel, 1999] ⁽¹⁾	r	$2\mu m$	$50nm$	$70nm$	$11nm$	
	ϵ	60	3	60	3	
	σ	$0.44\frac{S}{m}$	$0.1\frac{mS}{m}$	$25-185\frac{mS}{m}$	$2.5\frac{mS}{m}$	
[Hölzel, 1999]	r	$2.124\mu m$	0	$70nm$		
	ϵ	60		60		
	σ	$0.44\frac{S}{m}$		$6\frac{mS}{m}$		
	c	0	$15\frac{mF}{m^2}$	0	$30\frac{mF}{m^2}$	
	g	0	$2.5\frac{mS}{m^2}$	0		
[Hölzel, 1997] ⁽²⁾	r	$3\mu m$	$3.5nm$	$25nm$	$110nm$	$50nm$
	ϵ	51	3	14.4	60	5.9
	σ	$1.2\frac{S}{m}$	$2.9-3.7\frac{\mu S}{m}$	$4.1\frac{mS}{m}$	$2.9-24\frac{mS}{m}$	$20\frac{mS}{m}$
[Hölzel, 2002] ⁽³⁾	r	$3.2\mu m$	$3.5nm$	$30nm$	$175nm$	$115nm$
	ϵ	150	3	13	65	5.5
	σ	$0.3-1.4\frac{S}{m}$	$0.58\frac{\mu S}{m}$	$1.1\frac{mS}{m}$	$0.61\frac{mS}{m}$	$10\frac{mS}{m}$

Table 3.1: Model parameters for the simulation shown in figure 3.1. Shells with a certain thickness have the parameters radius r , relative permittivity ϵ_r and conductivity σ . Thin layers are modeled with an effective capacitance c_m and a conductance g_m , both per unit surface area.

(1) σ for the 2nd shell is $25\frac{mS}{m}$, $90\frac{mS}{m}$, and $185\frac{mS}{m}$ for a medium conductivity of $0.015\frac{S}{m}$, $0.15\frac{S}{m}$, and $1.5\frac{S}{m}$, respectively.

(2) σ for the 1st shell is $2.9\frac{\mu S}{m}$, $4.6\frac{\mu S}{m}$, and $3.7\frac{\mu S}{m}$ for a medium conductivity of $2\frac{mS}{m}$, $9\frac{mS}{m}$, and $55\frac{mS}{m}$, respectively.

σ for the 3rd shell is $2.9\frac{mS}{m}$, $6.2\frac{mS}{m}$, and $24\frac{mS}{m}$ for a medium conductivity of $2\frac{mS}{m}$, $9\frac{mS}{m}$, and $55\frac{mS}{m}$, respectively.

(3) σ for the cytoplasm is $0.3\frac{S}{m}$, $0.9\frac{S}{m}$, and $1.4\frac{S}{m}$ for a medium conductivity of $1\frac{mS}{m}$, $20\frac{mS}{m}$, and $100\frac{mS}{m}$, respectively.

3.3 Electric field simulation

COMSOL Multiphysics is a powerful simulation software capable of computing complex physical problems based on the finite element method. In a graphical editor 2D as well as 3D models can be created and subdomain and boundary conditions can be specified. Predefined systems of equations can be applied to solve common physical problems like *Incompressible Navier Stokes* flow and *Electric Currents* that were used in this work. This section gives a short introduction in the manual creation of a 2D model for simulating a part of the separation channel. The actual optimization of the geometry of one section of the separation channel, the so called DEP unit, was then done in an automated way with MATLAB as explained in section 3.6.

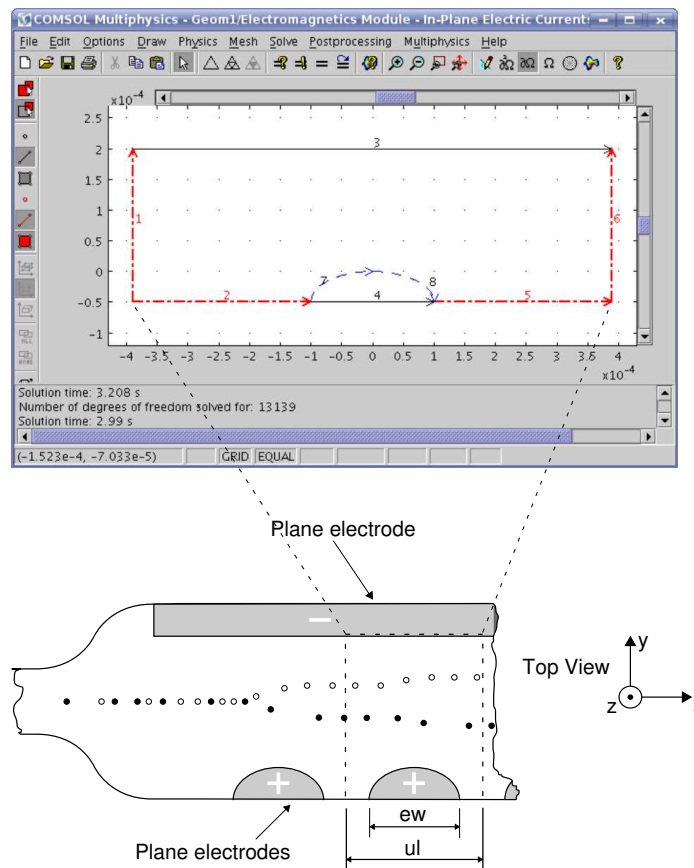


Figure 3.2: Model of a DEP unit in COMSOL with boundary numbering

Figure 3.2 shows the COMSOL model of one DEP unit. The actual electrode is not modeled here but only the outlines are drawn. Boundary 4 is not needed for the electric field simulation but will be used in the fluid flow simulation to define the channel boundary. The voltages of the electrodes are specified as conditions at the corresponding boundaries. It is important to notice that due to the 2D simulation the electrodes are not treated as plane

electrodes and the channel is not treated as if it has a certain height. The structure is considered as if it has an endless extension normal to the drawing area. This is adequate for the optimization process as long as particles do not leave a certain *separation zone* shown in figure 1.1. This simplification is described in section 3.5. Because the real electrode is plane the voltage that needs to be applied is slightly higher than used in the 2D simulation to result in the same particle deviation.

Constants are defined in the dialog box *Options* → *Constants...* according to table 3.2 that additionally contains entries for the fluid flow simulation in the next section. After selecting the application mode *ElectromagneticsModule* → *Quasi – Statics, Electric* → *In – PlaneElectricCurrents* in the *Multiphysics* → *ModelNavigator...* dialog box the subdomain and boundary conditions can be specified according to table 3.3, table 3.4.

Name	Expression
V_electrode	1
v_medium	1e-3
rho_medium	1050
epsr_medium	80
sig_medium	1.5e-2
eta_medium	0.997e-3
r_Y	2.5e-6
K_Y	0.7
k1_Y	4*pi*eta_medium*r_Y
r_EC	0.5e-6
K_EC	-0.3
k1_EC	4*pi*eta_medium*r_EC

Table 3.2: Simulation constants

Subdomain	Quantity	Expression
1	σ (isotropic)	sig_medium
	ε (isotropic)	epsr_medium
	d	30e-6
2	In-Plane Electric Currents not active in this domain	

Table 3.3: Subdomain settings for application mode *In-Plane Electric Currents*

In the dialog box *Options* → *Expressions* → *SubdomainExpressions* subdomain expressions are defined as shown in figure 3.5 to ease the postprocessing task. Then, for example, the dielectrophoretic force acting on bakers yeast can easily be plotted by using the expressions $Fdexp_X$ and $Fdexp_Y$.

In figure 3.3 the surface plot for the electric potential and the arrow plot for the dielectrophoretic force acting on yeast is shown using the previous mentioned expressions.

Boundary	Condition	Quantity	Value
1, 2, 5, 6	Electric insulation	<i>predefined</i>	
3	Ground		
4	- (not set since In-Plane Electric Currents is inactive in subdomain 2)		
7, 8	Electric potential	V_0	$V_{\text{electrode}}$

Table 3.4: Boundary settings for application mode *In-Plane Electric Currents*

Name	Expression
Fdep _{x0}	$2 \cdot \pi \cdot \epsilon_{\text{medium}} \cdot \text{diff}(\text{normE}_{\text{emqvw}}^2, x)$
Fdep _{y0}	$2 \cdot \pi \cdot \epsilon_{\text{medium}} \cdot \text{diff}(\text{normE}_{\text{emqvw}}^2, y)$
Fdep _{x_Y}	$F\text{dep}_{x0} \cdot r_Y^3 \cdot K_Y$
Fdep _{y_Y}	$F\text{dep}_{y0} \cdot r_Y^3 \cdot K_Y$

Table 3.5: Subdomain expressions for application mode *In-Plane Electric Currents*

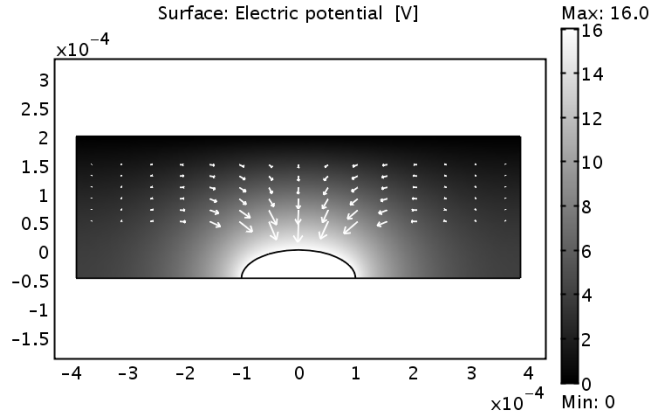


Figure 3.3: Postprocessing result for electric potential and dielectrophoretic force acting on bakers yeast

The inhomogeneity of the electric field increases from the straight electrode to the round electrode, so the DEP force represented by the arrows points to the round electrode. That means that particles that are present in the DEP unit would be attracted by that electrode.

3.4 Fluid flow simulation

To achieve a continuous separation a second force, beside the DEP force, is needed to move the particles past the inhomogeneous electric field that was simulated in the previous section. This second force is the drag force produced by a fluid flow.

In addition to *In-Plane Electric Currents* a second application mode is needed to simulate the fluid flow for the calculation of the drag force acting on the particles. Therefore the application mode *MEMSModule* \rightarrow *Microfluidics* \rightarrow *GeneralLaminarFlow* is applied via the model navigator. The necessary constants have already been defined in the previous section. Subdomain settings, boundary settings, and additional subdomain expressions are summarized in table 3.6, table 3.7, and table 3.8, respectively.

Subdomain	Quantity	Expression
1, 2	ρ	rho_medium
	η	eta_medium
	Thickness	30e-6
	Checkbox	<i>Add shallow channel approximation</i> has to be activated

Table 3.6: Subdomain settings for application mode *General Laminar Flow*

Boundary	Condition	Quantity	Value
1	Laminar Inflow	U_0	v_medium
2, 3, 4, 5	No slip	<i>predefined</i>	
6	Outflow/Pressure		
7, 8	Neutral		

Table 3.7: Boundary settings for application mode *General Laminar Flow*

Name	Expression
Ffluidx_Y	k1_Y*u
Ffluidy_Y	k1_Y*v
Fx_Y	Fdep _x _Y+Ffluidx_Y
Fy_Y	Fdep _y _Y+Ffluidy_Y

Table 3.8: Subdomain expressions for application mode *General Laminar Flow*

Figure 3.4 shows the postprocessing result of the simulation for the trajectories of particles starting at position $y = 100^{\pm 5} \mu m$. The combination of DEP force and drag force deviates the particles depending on their Clausius Mossotti factor and size.

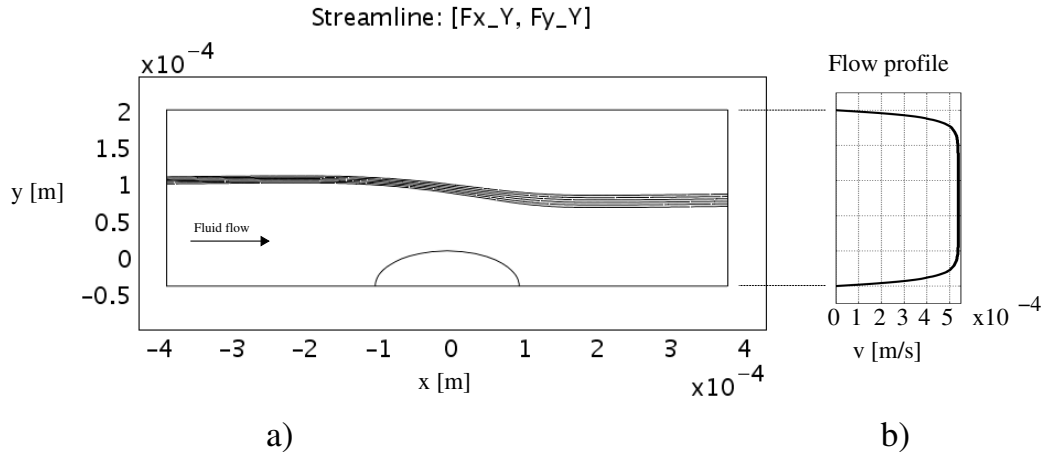


Figure 3.4: Particle trajectories for bakers yeast (a) and fluid flow profile (b) for the simulation of DEP force and drag force. The flow profile shows that the fluid velocity can be considered as constant in the horizontal axis in the *separation zone*.

3.5 Simplifications for the simulation

The simulation of a complex model in three dimensions may be problematic. Especially when applying the finite element method to multiple physical models in a mesh with high resolution the calculating capacity is a limiting factor. Therefore it is important to simplify the existing model and to automate the calculation of the model behaviour for varying model parameters. The following simplifications can be applied to the simulation and optimization process without losing relevant information:

- Figure 3.5 a) shows that the isosurface planes of the electric potential are parallel in the middle part of the separation channel. Therefore the electric field is independent of the vertical position in that middle part and the simulation for the electric field can be reduced to a two dimensional calculation in the x-y plane.
- Since the separation takes place in the y-direction in the middle part of the channel the simulations were carried out with a constant fluid velocity (figure 3.5 b). The optimal electrode configuration is independent of the fluid velocity and thus of the particle velocity.
- The separation channel is made up of several equal designed DEP units. Therefore the method of mirror charges can be applied because the electrode charges can be mirrored at the meeting faces of two DEP units where the isosurface planes of the electric potential are crossing orthogonally, see figure 3.6. An explanation of the method for mirror charges can be found in [Dirschmid, 1992, p. 1275]. This way not the whole channel but only one DEP unit has to be simulated and the result can then be processed in MATLAB and a whole channel can be calculated by stringing together several single units.

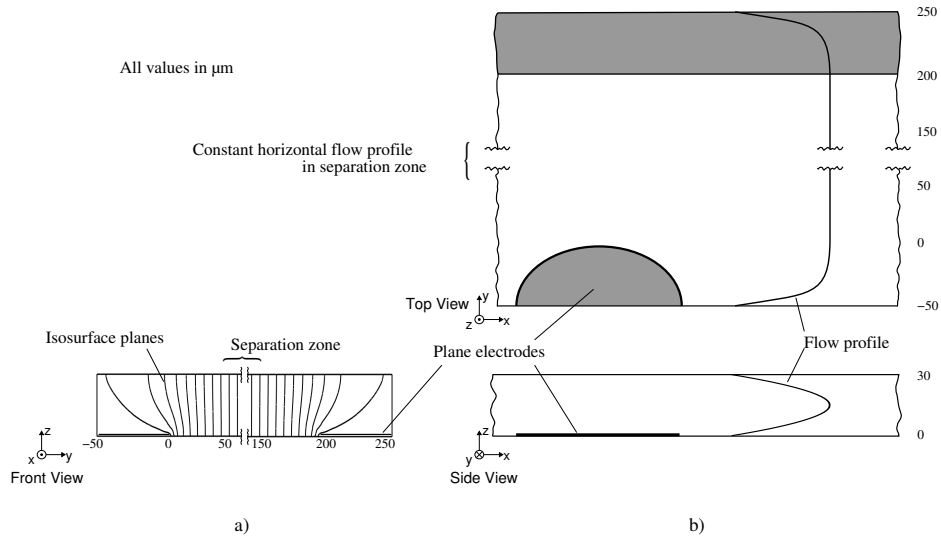


Figure 3.5: Simplifications can be made for the simulation of the (a) electric field and (b) fluid flow profile

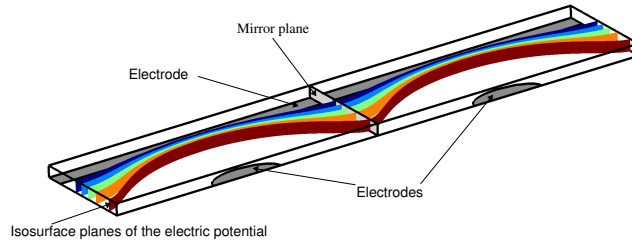


Figure 3.6: Method of mirror charges is applied to the indicated mirror plane so only one DEP unit has to be simulated.

3.6 Optimization of electrode geometry in 2D

The purpose of the simulation is to predict the particle movement in the device due to the microfluidic flow and the dielectrophoretic force in order to optimize the geometry of the electrodes. That optimization is done completely in MATLAB, including the automated simulation of the DEP units of varying dimensions via COMSOL. This section describes the implementation of this optimization automatism.

The integration of COMSOL in MATLAB makes it possible to control the modelling, calculation, and postprocessing tasks of COMSOL programmatically out of MATLAB. The simulation data can be retrieved and further calculations can then be done in MATLAB. For this purpose COMSOL uses a so called *fem*-structure which contains all data related to a specific simulation including geometry, application mode settings, simulation results, and

postprocessing settings. A shortened but fully functional version of the MATLAB scripts can be found in appendix A.

The optimization is based on the calculation of particle trajectories for varying electrode geometries whereas the other parameters are held constant. The major difficulty is to determine the parameters that should be varied because the more parameters the simulation depends on the more complex the optimization gets. Therefore the optimization carried out in this work is based on two design parameters shown in figure 3.7. The optimal values for ul and ew are independent of the other parameters like particle size, supply voltage or fluid velocity but depend on the width of the separation channel.

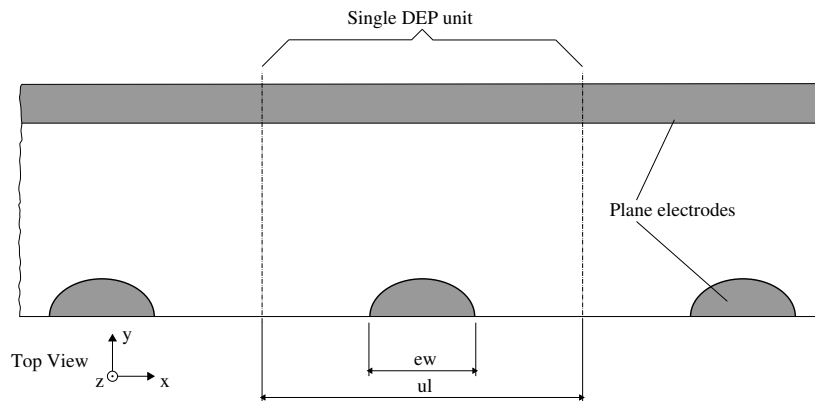


Figure 3.7: Design parameters DEP unit length (ul) and electrode width (ew) the optimization depends on.

Figure 3.8 shows the program flow for the optimization process that will be explained in the next paragraph.

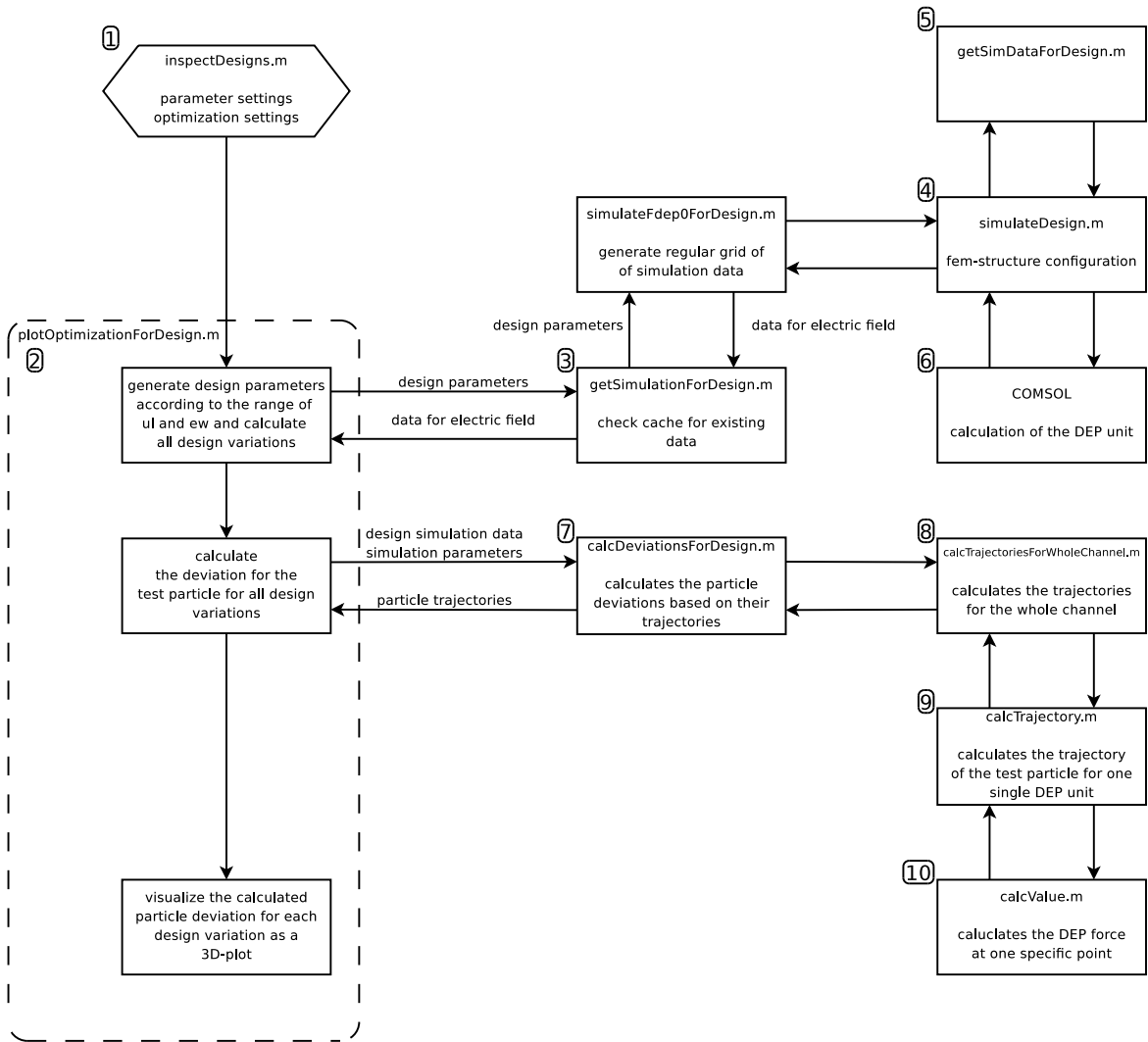


Figure 3.8: Program flow for the geometry optimization of a device with a certain channel width and electrode shape

- 1 The file *inspectDesigns.m* is the start point for the optimization process. Herein the following fixed optimization parameters are configured:

timestep Defines the accuracy of simulation. The smaller the timestep the more accurate and computationally intensive the simulation result will be, see figure 2.5.

v_medium The slower the fluid moves the longer are the particles exposed to the dielectrophoretic force field.

U_electrode The voltage that is applied to the electrodes.

particle Particle parameters like radius and Clausius Mossotti factor which should be used for the optimization.

channel width (cw) For an optimization the channel width is predefined because this

parameter depends on the particle size, available supply voltage and particle focussing quality.

startpoint The startpoint of the test particle.

rangeMinMaxY Defines the separation zone that the particle must not leave during the separation process, otherwise the optimization has to be aborted.

whole channel length the whole length of the separation channel that should be used for calculation of the particle deviations. Too short channel length lead to an imprecise result, on the other hand a too long channel demands more calculation time.

As mentioned before the optimization is based on two design parameters that are varied during the optimization which are

ul The DEP unit length which varies in a certain range.

ew The electrode width which varies in a certain range.

- 2 The file *plotOptimizationForDesign.m* first calls *getSimulationForDesign.m* for every design variation which is specified with the *ul* and *ew* parameters.
- 3 The file *getSimulationForDesign.m* implements a caching functionality that first tries to load the simulation data from a previously stored file. If such a file does not exist the file *simulateFdep0ForDesign.m* is called. The caching mechanism is based on the fact that starting from a dielectrophoretic force field produced by a voltage of 1V the force field for every voltage can be calculated simply by multiplying with U^2 (see equation 2.8). The same simplification applies to the Clausius Mossotti factor and the particle radius. Therefore the following functions do not calculate F_{DEP} but rather F_{DEP_0} as shown in table 3.5.
- 4 The file *simulateFdep0ForDesign.m* uses the COMSOL function *posteval* to calculate F_{DEP_0} in a regular Grid that can be used in the file *calcValue.m* to interpolate required values much more easier since the mesh generated by COMSOL is irregular and adapted to the electrode geometry. To get the simulation data it calls
- 5 the file *simulateDesign.m*. This function configures the *fem*-structure that is used by COMSOL. It sets constants, application mode, subdomain expressions and solver. The geometry is created by
- 6 *getSimDataForDesign.m*. Depending on the requested design type, DEP unit and electrode dimensions a geometry object is returned that can directly be used with the *fem*-structure.

Afterwards the file

- 7 *calcDeviationsForDesign.m* is called. It calculates the trajectory data for the whole channel for each design that has been simulated previously using the next function.
- 8 In the function *calcTrajectoriesForWholeChannel.m* as much DEP units as needed for the specified channel length are arranged successively and the trajectory for the given particle is calculated. The starting point of the particle in a DEP unit

is the endpoint of the trajectory in the previous unit. The trajectory in a single DEP unit is calculated in

- 9) the file *calcTrajectory.m*. The trajectory of a particle in one single DEP unit is determined by calculating the particle velocity at the actual position and multiplying it with the specified timestep. The result is a displacement leading to the next point of the trajectory. The DEP force at a certain point is interpolated using the function
- 10) *calcValue.m*. It calculates the value of the DEP force using a linear interpolation that considers the four nearest grid points according to equation 3.1 and figure 3.9.

Then the deviation for each *ul* and *ew* combination is visualized in a 3D-plot and the maximum deviation can easily be determined, see figure 3.10.

$$F_x = (F_{x(i,j)} \cdot (1 - w_x) + F_{x(i,j+1)} \cdot (w_x)) \cdot (1 - w_y) + (F_{x(i+1,j)} \cdot (1 - w_x) + F_{x(i+1,j+1)} \cdot (w_x)) \cdot (w_y) \quad (3.1)$$

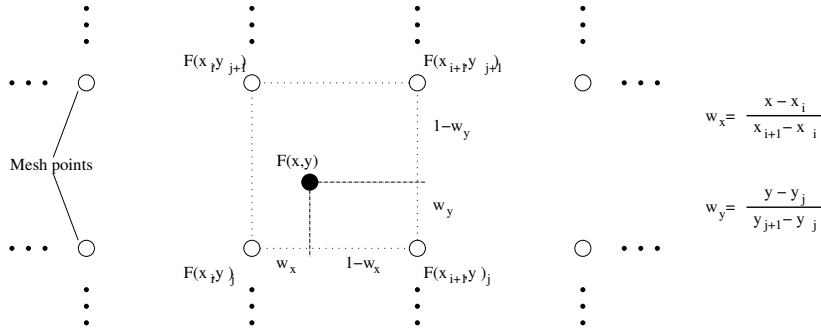


Figure 3.9: The value for the force at a certain point is the result of a linear interpolation of the values at the four nearest grid points using equation 3.1

The result for an optimization process with the parameters summarized in table 3.9 is shown in figure 3.10.

Name	Expression
V_electrode	8V
v_medium	1e-3 m/s
eta_medium	1.030e-3
r_Y	2.5e-6
K_Y	0.7
timestep	0.001s
range_ul	600..1000\mu m
range_ew	100..300\mu m

Table 3.9: Parameters for the optimization shown in figure 3.10.

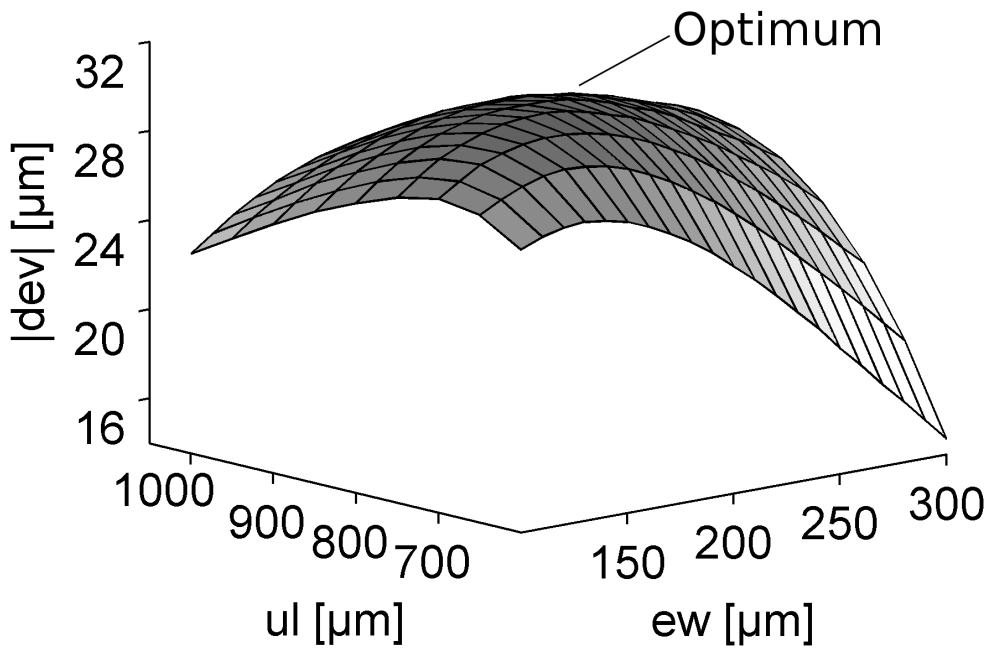


Figure 3.10: The result for the optimization with the parameters shown in table 3.9. The design geometry for the maximum deviation of $30\mu\text{m}$ is $ul = 780\mu\text{m}$ and $ew = 200\mu\text{m}$.

It is important to note that the velocity of the fluid is a predefined parameter in this optimization because the velocity is according to figure 3.4 constant in the separation zone. Additionally the optimal electrode dimensions are independent of the fluid flow velocity as shown by optimizations which were conducted with differing velocities. That is obvious since the direction of particle deviation and fluid motion are perpendicular and therefore

independent from each other.

Parameter	Value
ul	$780\mu m$
ew	$200\mu m$

Table 3.10: Optimized values for DEP unit length and electrode width with a given separation zone width of $100\mu m$ as a result of the optimization process shown in figure 3.10. As a rule of thumb for that shape of the small electrode the width of the electrode ew has to be equal to the distance between the long electrode and the small electrodes and the DEP unit length ul should be four times the electrode width ew .

The optimization process leads to the the optimal values shown in table 3.10.

It is not necessary to repeat the whole optimization process for other channel widths because the optimal design geometry can be down- or upscaled to fabricate devices of alternative dimensions.

3.6.1 Plotting trajectories for optimized design geometry

Using the script *inspectDesigns.m* the trajectories of different particles can be plotted in a very convenient way. In contrast to the steps needed for the optimization described in the previous section now only one design has to be simulated. That is done directly in the script *inspectDesigns.m*. Then the trajectories are plotted calling the function *plotTrajectoriesForWholeChannel* which uses function *calcTrajectoriesForWholeChannel*, explained in the previous section, to calculate the trajectories for the specified particles. The only thing left is to draw a nice figure for the particle trajectories like the one shown in figure 3.11 with the particle parameters summarized in table 3.11.

Name	Expression
r_{EC}	$1e-6$
K_{EC}	-0.3

Table 3.11: Additional parameters for the particle trajectories plot shown in figure 3.11. The other simulation parameters are shown in table 3.9.

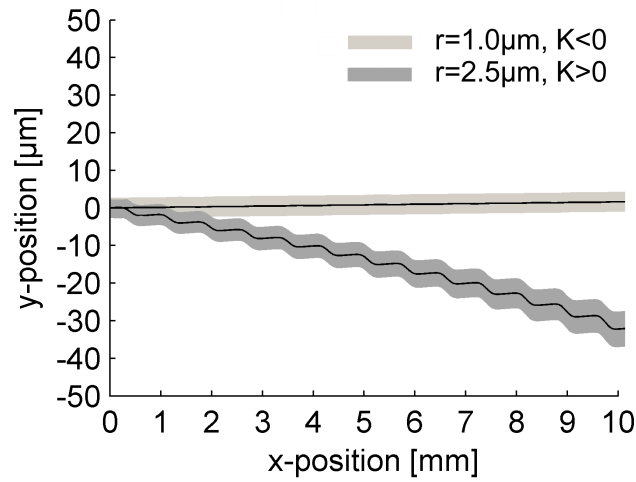


Figure 3.11: The simulated particle trajectories with the parameters shown in table 3.11.

3.7 Verification of the simulation results in 3D

To verify the simulation results of the 2D simulation additionally a 3D model of a DEP unit is modeled and simulated. It is expected that the deviation of a particle is slightly smaller in 3D than in 2D since the electrodes are plane electrodes now and a higher voltage is needed to create the same field in the separation zone as in 2D.

In figure 3.12 the simulation results are superimposed to illustrate the differing trajectories.

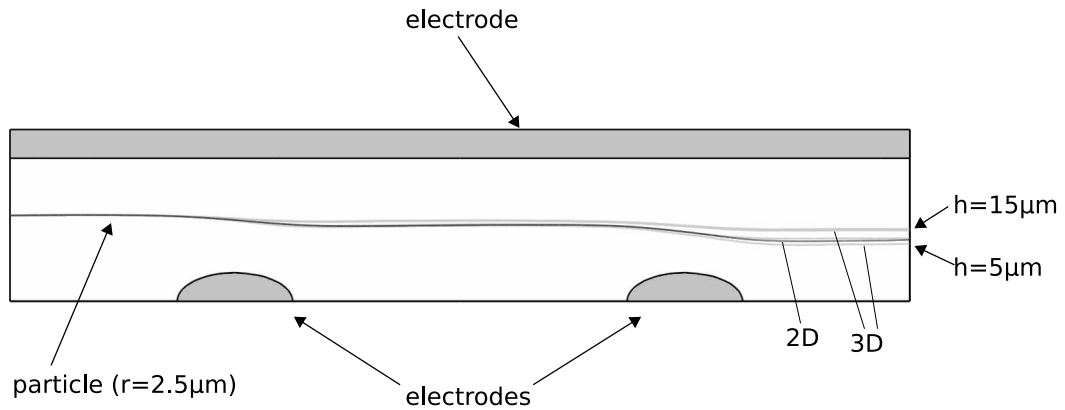


Figure 3.12: The simulations in 2D (black line) and in 3D (gray lines) are superimposed to illustrate the different results of these two simulation methods. The gray lines are the trajectories of particles moving at different heights. Due to the parabolic flow profile the particles near the top and bottom of the channel are moving slower and so they are exposed to the dielectrophoretic force for a longer time. To realize the same deviation in 3D as in 2D a slightly higher voltage (17.5V instead of 14V for this simulation parameters) is required because in 3D the electrodes are plane electrodes so the difference of potential in the separation zone is less.

4 Device

4.1 Introduction

In this chapter the fabricated device and the considerations which led to the chosen design are presented.

Section 4.2 describes practical considerations that had to be taken into account. That includes the particle behavior in the flow channel, heating due to electrical losses, and electrode erosion.

In section 4.3 the concept of the device in all its parts is presented including the particle injection, focusing, separation, and the implemented method of evaluation of the particle deviation efficiency. Additionally in that section the considered separation principles are briefly introduced and their pros and cons are discussed.

Then the prerequisites and restrictions for the device, like geometry limitations, are covered in section 4.4.

Finally the actual fabrication process of the device is explained in section 4.5 and photographs of the fabricated device are included at the end of this chapter.

4.2 Practical considerations

When a new device concept is realized a number of secondary effects have to be considered that accompany and even may influence the actual function negatively. The side effects that were considered in this work are presented in this section.

4.2.1 Particle sedimentation

The sedimentation of particles can be a serious problem in microfluidic devices. Therefore it is important to estimate the influence of buoyancy and gravity force on the particle movement. To accomplish this equation 2.30 is applied to the particles and fluids used. The device will be tested both with polymer particles in deionized water and biological organisms, namely bakers yeast and E. coli bacteria, in 0.4M mannitol solution. The physical properties are summarized in table 4.1.

The mass of mannitol and deionized water in 1cm^3 of 0.4M mannitol solution at 25°C is

type	$\rho \left[\frac{g}{cm^3} \right]$ 25°C	$\rho \left[\frac{g}{cm^3} \right]$ 35°C	$\varnothing [\mu m]$	$\eta [mPa \cdot s]$ 25°C	$\eta [mPa \cdot s]$ 35°C
polymer bead	1.03	1.03	1, 5	-	-
bakers yeast	$\sim 1^{(1)}$	$\sim 1^{(1)}$	5	-	-
E. coli	$\sim 1^{(1)}$	$\sim 1^{(1)}$	1	-	-
deionized (DI) water	0.997	0.994	-	0.8904	0.7196
0.4M mannitol	1.021	1.018	-	1.03	0.8324

Table 4.1: Physical properties of particles and solutions used in the measurements. The values for ⁽¹⁾ were taken out of [Fritsche, 1999, p. 46]

$$m_M = 0.001 dm^3 \cdot 0.4 \frac{mol}{dm^3} \cdot 182.17 \frac{g}{mol} = 0.0729g \quad (4.1)$$

$$V_M = \frac{m_M}{\rho_M} = \frac{0.0729g}{1.49 \frac{g}{cm^3}} = 0.0489cm^3 \quad (4.2)$$

$$V_{H_2O} = 1cm^3 - 0.0489cm^3 = 0.951cm^3 \quad (4.3)$$

$$m_{H_2O} = \rho_{H_2O} \cdot V_{H_2O} = 0.997 \frac{g}{cm^3} \cdot 0.951cm^3 = 0.9481g \quad (4.4)$$

where m_M , V_M , and ρ_M are the mass, volume, and mass density of mannitol, respectively, and m_{H_2O} , V_{H_2O} , and ρ_{H_2O} are the mass, volume, and mass density of deionized water, respectively. The density of that solution at 25°C is

$$\rho_{0.4M} = \frac{m_M + m_{H_2O}}{1cm^3} = \frac{0.0729g + 0.9481g}{1cm^3} = 1.021 \frac{g}{cm^3}. \quad (4.5)$$

For the density at 35°C the density of deionized water has to be replaced by $0.994 \frac{g}{cm^3}$. The density of mannitol is considered to be constant.

With these values the sedimentation velocity v_p is calculated according to equation 2.30 and the results are shown in table 4.2.

solution	particle	$v_p \left[\frac{\mu m}{s} \right]$ 25°C	$v_p \left[\frac{\mu m}{s} \right]$ 35°C
DI water	polystyrene bead (1 μm)	0.020	0.027
DI water	polystyrene bead (5 μm)	0.504	0.682
0.4 mannitol	bakers yeast (5 μm)	-0.278	-0.295
0.4 mannitol	E. coli (1 μm)	-0.011	-0.018
0.4 mannitol	polystyrene bead (1 μm)	0.0048	0.0079
0.4 mannitol	polystyrene bead (5 μm)	0.12	0.196

Table 4.2: Sedimentation velocity for different solution-particle combinations

According to section 4.3.1 the minimum flow speed in the separation channel will not be below 1 mm/s and the time a particle needs to pass the separation channel will not be more

than 10s. So the maximum vertical displacement according to table 4.2 is about $7\mu m$. If the particles are suspended in 0.4 mannitol solution only the maximum displacement is decreased to about $3\mu m$ and can therefore be neglected.

4.2.2 Joule heating

Joule heating is the result of electric currents flowing through conductors. Since the fluid where the particles are suspended in has a certain conductivity the voltage applied to the electrodes produces an electric current and therefore a non negligible heat in the suspension. Additionally the conductivity of the substrate makes an impact at higher frequencies where the insulating impedance of the nitride layer decreases.

4.2.2.1 Joule heating in the suspension

The heating effect in the suspension is simulated in COMSOL Multiphysics for a single DEP unit using the application modes *General Laminar Flow*, *Electric Currents*, and *General Heat Transfer*. The first two modes are known from the simulation chapter, the latter one is needed to simulate the transfer of the heat produced by the supply voltage to the fluid. The conductive and convective heat flux in the moving fluid caused by the resistive heating is calculated and boundary integrations for the temperature at the inlet and outlet of the DEP unit are performed. The difference between these two temperatures can be used to calculate the temperature rise in a channel of a certain length. The results for the joule heating simulation for a DEP unit with the dimensions optimized in the previous chapter are summarized in table 4.3. The measurement of the electric conductivity of the suspension is described in section 4.2.4.

4.2.2.2 Joule heating in the substrate

The silicon substrate has a conductivity of about $20 - 50 \frac{S}{m}$. The standard isolating layer between the electrodes and the substrate is made up of $250\text{ nm } SiO_2$ ($\epsilon_r = 3.9$) and $70\text{ nm } Si_3N_4$ ($\epsilon_r = 7.5$). At higher frequencies the impedance of this layer decreases and losses arise in the substrate. A test device without microfluidic channels was fabricated that was used to measure the impedance Z between the electrodes over the frequency with a network analyzer. The power dissipation against the frequency can now be calculated for a specific electrode voltage. A very simplified model for the impedance Z is shown in figure 4.1. The values for R , L , C , and P_{eff} were calculated using equations 4.6, 4.7, 4.8, and 4.9.

Parameter	Value	Unit	Comment
U	18	V	electrode voltage
v	1	$\frac{mm}{s}$	velocity of suspension
ρ	1.021	$\frac{g}{cm^3}$	mass density of suspension
σ	13	$\frac{\mu S}{m}$	electric conductivity of suspension
η	1.03	$mPa \cdot s$	dynamic viscosity of suspension
C_p	4183	$\frac{J}{kg \cdot K}$	heat capacity of suspension
k_m	0.6	$\frac{W}{m \cdot K}$	thermal conductivity of suspension
ch	30	μm	channel height
cl	780	μm	channel length of one DEP unit
ew	200	μm	electrode width
ΔT (DEP unit)	0.27	K	increase of temperature
ΔT (10mm)	3.5	K	increase of temperature

Table 4.3: Simulation parameters and results for joule heating of 0.4M mannitol suspension used for the experiments with biological cells. The simulation was performed for the worst case with thermal isolation at the channel boundaries, the maximum applicable voltage, and the maximum channel length that was realized. That means that an increase of temperature is expected that is less than $3.5K$

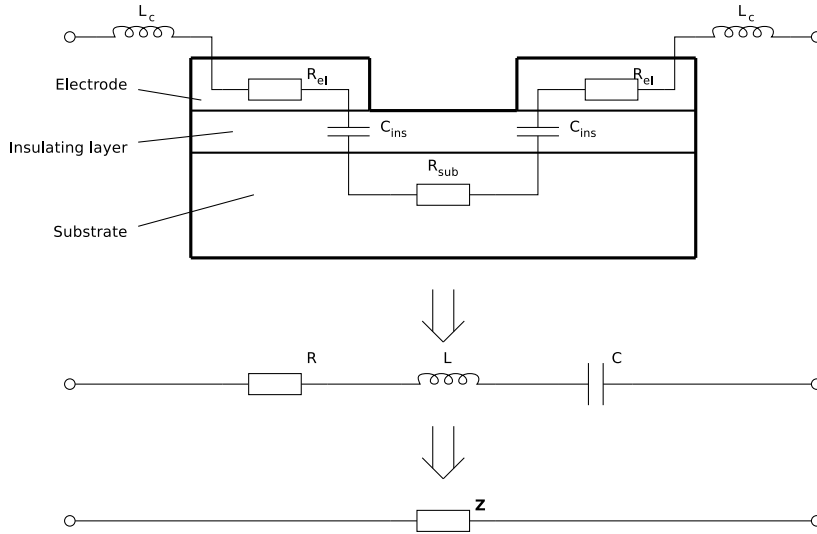


Figure 4.1: A simple model for the impedance of the electrodes, insulating layer, and substrate. The resistances, inductances, and capacitances are combined to the single components R , L , and C .

$$Z = R + \frac{1}{j\omega C} + j\omega L$$

$$R \approx |Z(f = f_r)| \quad (4.6)$$

$$C \approx \frac{1}{\omega \cdot \Im[Z]} \quad \text{at the frequency } f_{-90^\circ} \ (\varphi = -90^\circ) \quad (4.7)$$

$$L \approx \frac{1}{(2\pi f_r)^2 \cdot C} \quad (4.8)$$

$$P = \frac{|U|^2}{|Z|} \cdot \cos(\varphi) \quad (4.9)$$

where f_r is the resonance frequency where $\varphi = 0^\circ$. Since a significant heating of the test device at the maximum available voltage and at frequencies over 1 *MHz* were noticed the final devices were fabricated with an additional insulation layer of 800 *nm SiN_x*. The measurements were repeated with the final device, including the microfluidic channels, and compared to the results from the test device.

Figure 4.2 shows the measurement results for Z and the calculated effective power dissipation P_{eff} for a supply voltage $U_{eff} = 18$ *V* for the long design, see section 4.4.2. The calculated values for R , L , C , and P_{eff} are summarized in table 4.4.

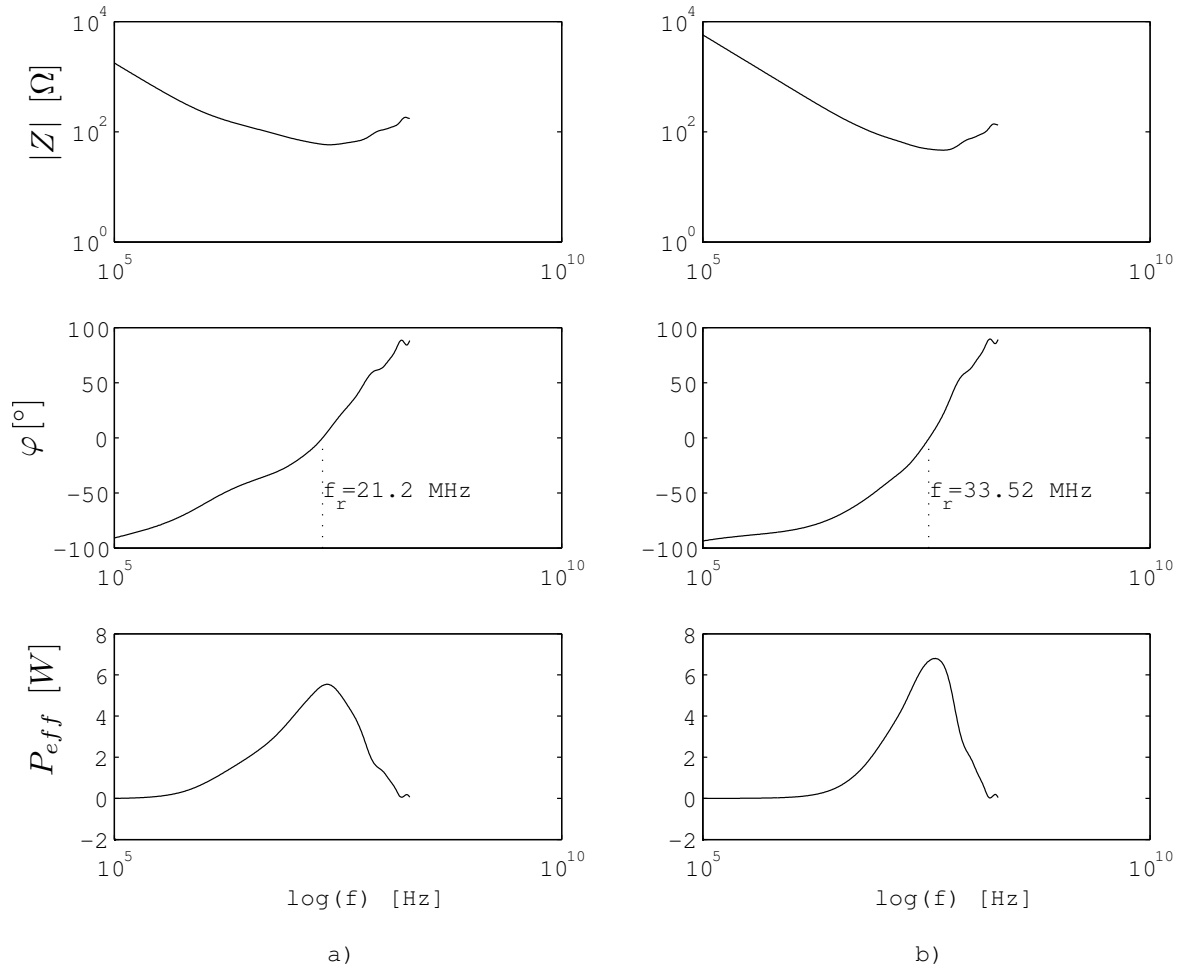


Figure 4.2: The impedance Z and the effective power dissipation P_{eff} for a supply voltage $U_{eff} = 18 V$ is shown for the test device without additional insulating layer on the left (a) and for the actual devices with the insulating layer of $800 \text{ nm } SiN_x$ on the right (b). The insulation layer decreases the capacitance between the electrodes and the substrate and therefore increases the resonance frequency from $f_r = 21.2 \text{ MHz}$ to $f_r = 33.52 \text{ MHz}$.

Parameter	w/o 800 nm SiN_x	with 800 nm SiN_x	Unit
R	59	48.6	Ω
L	2.48	3.2	μH
C	0.89	0.2738	nF
$P_{eff}(f = 1MHz)$	0.732	0.0614	W

Table 4.4: Calculation results of the combined values R , L , and C for the impedance of the power connection, electrodes, insulation, and substrate. The value of C decreases with the factor 3.25 which corresponds to the theoretical decrease of about 3.5 based on the ratio between the insulating layer thicknesses 1120 nm (*including* 800 nm SiN_x) and 320 nm. The effective power dissipation decreases with a factor of 12.

4.2.3 Electrode erosion

Electrode erosion or corrosion occurs if the metal is exposed to an electrolyte and a direct or low-frequency current is applied. Therefore platinum has been chosen as the electrode material since it is most resistant to corrosion. The rate of corrosion depends on the current density that flows out perpendicular to the metal surface. To counteract electrode erosion the number of corners and edges should be reduced to a minimum so the geometry of the small electrode has nearly the form of a isosurface plane of the electric potential of a point charge, see figure 4.3. As optimization runs for other electrode geometries pointed out the distance between the small electrodes is more important than the shape of the electrode itself.

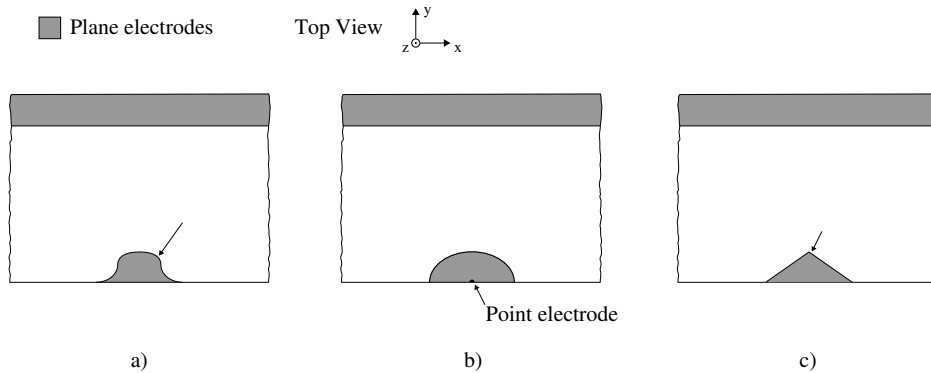


Figure 4.3: The chosen form of the small electrode in a single DEP unit is shown in b). It corresponds to the form of a isosurface plane of the electric potential of a point charge to minimize peaks of the electric current density. An optimization run was carried out with the result that the other electrode geometries in a) and c) show equal or less efficiency for the particle deviation. The arrows indicate the critical areas where erosion is likely to occur.

4.2.4 Suspension properties

A 0.4M mannitol solution is used as the suspension for the biological cells because of its low conductivity, see [Suehiro et al., 2001] and [Fatoyinbo et al., 2005]. Saline solution (0.9M NaCl) can not be used because of its high conductivity of about $1.5 \frac{S}{m}$ and the resulting electrode erosion at low voltages and frequencies. Table 4.5 summarizes the physical and electrical properties that are used in this work for 0.4M mannitol solution.

Parameter	Value	Unit	Comment
ρ	1.021	$\frac{g}{cm^3}$	mass density, see equation 4.5
σ	13	$\frac{\mu S}{m}$	electrical conductivity ⁽¹⁾
ϵ	78	–	relative permittivity
η	1.03	$mPa \cdot s$	absolute viscosity ⁽²⁾

Table 4.5: Physical and electrical properties of 0.4M mannitol solution used in this work.

⁽¹⁾ measured in a conductivity measuring cell with platinum electrodes according to equation 4.11.

⁽²⁾ measured with a viscometer.

The conductivity was measured with a conductivity measuring cell. The values were measured at a frequency of 2 MHz. The cell constant C was calculated using saline solution as a reference fluid:

$$\begin{aligned}
 R_{NaCl} &= 360\Omega \quad (\text{measured}) \\
 \sigma_{NaCl} &= \frac{1}{360}S = \sigma_{NaCl_{spec}} \cdot \frac{A}{l} = \sigma_{NaCl_{spec}} \cdot \frac{1}{C} \\
 C &= \frac{\sigma_{NaCl_{spec}}}{\sigma_{NaCl}} = \frac{1.5 \frac{S}{m}}{\frac{1}{360}S} = 540 \frac{1}{m}.
 \end{aligned} \tag{4.10}$$

where R_{NaCl} is the measured resistance of the saline solution in the measuring cell. The measured resistance of the mannitol solution led to the specific conductivity $\sigma_{mannitol_{spec}}$

$$\begin{aligned}
 R_{mannitol} &= 400k\Omega \quad (\text{measured}) \\
 \sigma_{mannitol_{spec}} &= \frac{1}{R_{mannitol}} \cdot C = \frac{1}{400000 \frac{1}{S}} \cdot 540 \frac{1}{m} = 13 \frac{\mu S}{m}.
 \end{aligned} \tag{4.11}$$

Thanks to Mr. Markus Luchner the suitability of 0.4M mannitol solution for suspending bacteria was tested at the *University of Natural Resources and Applied Life Sciences, Vienna* with E. coli. In two hours only 0.2 % of the organisms died and on the other hand they did not grow too. That means that this solution is suited very well for the device tests.

4.3 Concept

In the next sections the individual parts of the device are presented. The fluid inlets, particle focusing, separation area, and detection area can be discussed independently from each other although every single part depends on the previous one.

4.3.1 Sample injection and particle focusing

The sample, sheath, and side port flows are injected into the device through the silicon substrate that acts as a carrier material for the microfluidic structures. Holes are etched into the substrate which serve as the inlets for the fluid. Figure 4.4 shows a cross-sectional view of the sample inlet and the resulting flow. The sample flow is directed to the taper via the sheath flow that additionally pushes the particles to the bottom of the channel to transport all the particles with almost the same velocity despite the fact that the gradient of the parabolic flow profile is larger at the bottom and top of the channel than in the center. If the particles would be spread over the whole channel height the variation of the particle velocities would be more than twice as much than for the particles travelling only in the lower region of the channel. The separation efficiency heavily depends on a constant flow velocity for all particles.

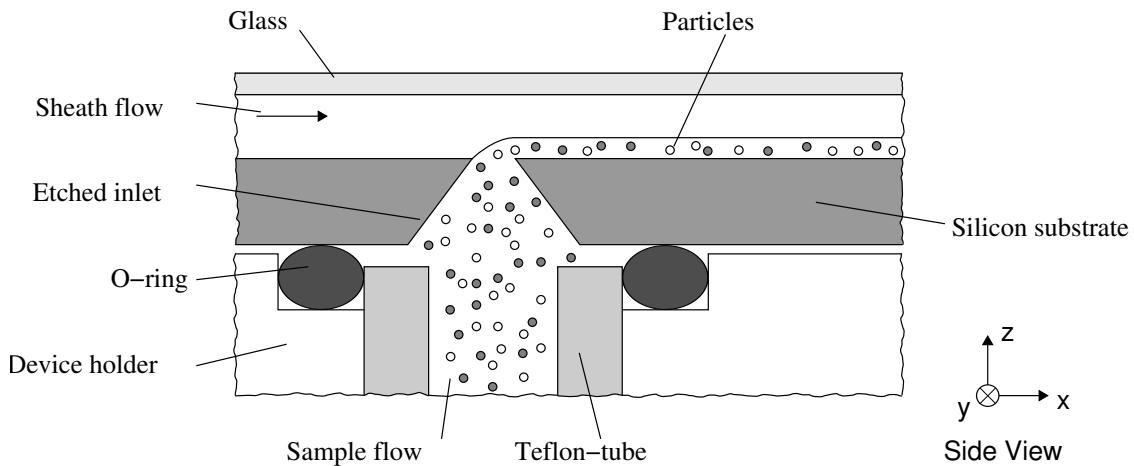


Figure 4.4: Cross-sectional view of the sample inlet. A syringe pump injects the particles via a teflon-tube through the inlet in the substrate into the microfluidic channel. The tube is plugged into a device holder made of DELRIN and an o-ring seals the connection between the holder and the device. This principle applies to the other inlets as well. For a description of the complete setup refer to section 5.1.

The idea for the separation process presented in this work assumes that the particles are centered before so that all of them enter the separation channel at the same position. The applied method to achieve this focusing is presented in [Nieuwenhuis, 2005, p.24]. As shown in figure 4.5 the particles enter the flow channel through the sample inlet and they are pre-focused with the taper before they are focused in the junction of the combined sheath

and sample flow and the side port flows. According to [Hang et al., 2005] the particles are arranged in a row if the width of the focused sample flow is smaller than the diameter of the suspended particles.

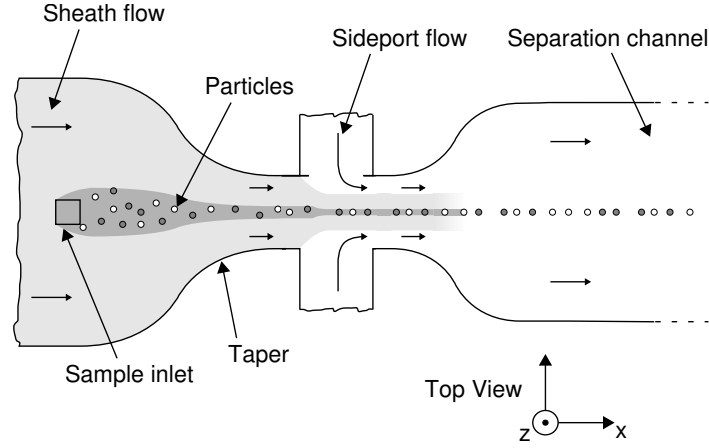


Figure 4.5: Top view onto the focusing part of the device. The particles enter the channel through the sample inlet and they are pushed into the taper by the sheath flow. The taper pre-focuses the sample flow for the second focus mechanism via the side port flows. When the particles enter the separation channel they should already be aligned in a row.

The experimental results for the optimal flow speed ratios are summarized in chapter 5. The main problem at low flow speeds is the clogging of the sample inlet with particles because a very dense sample is needed to rise the number of particles entering the channel in a certain time interval. The optimization showed that a flow speed of about 1 mm/s is needed in the separation zone. The corresponding flow rate for a channel width of $300 \mu\text{m}$ and height of $30 \mu\text{m}$ is calculated as follows:

$$\begin{aligned}
 V &= 300\mu\text{m} \cdot 30\mu\text{m} \cdot 1\text{mm} \cdot 1000 \frac{\text{l}}{\text{m}^3} = 9\text{nl} \\
 r_{SEP} &= 9 \frac{\text{nl}}{\text{s}} = 9 \frac{10^{-3}\mu\text{l}}{60^{-1}\text{min}} = 0.54 \frac{\mu\text{l}}{\text{min}}
 \end{aligned} \tag{4.12}$$

V is the volume in l that is moved within a second through a separation channel cross section. r_{SEP} is the flow rate in the separation channel. For a ratio of $1 : 5 : 10$ for the sample, side port, and sheath port flow, respectively, the theoretical values for the flow rates are summarized in equation 4.13 for a flow speed of 1 mm/s in the separation zone.

$$\begin{aligned}
r_{SA} + 2 \cdot r_{SP} + r_{SH} &= r_{SEP} \\
r_{SA} + 2 \cdot 5 \cdot r_{SA} + 10 \cdot r_{SA} &= r_{SEP} \\
r_{SA} &= \frac{r_{SEP}}{21} = \frac{0.54 \frac{\mu l}{min}}{21} = 0.0257 \frac{\mu l}{min} \\
r_{SP} &= 5 \cdot r_{SA} = 0.129 \frac{\mu l}{min} \\
r_{SH} &= 10 \cdot r_{SA} = 0.2571 \frac{\mu l}{min}
\end{aligned} \tag{4.13}$$

r_{SA} , r_{SP} , and r_{SH} are the flow rates for the sample, side port, and sheath inlets, respectively. The side port flow takes effect twice since there are two side port inlets.

Another problem may arise because of the rare steps of the syringe pumps at low flow rates even with syringes with a volume of 1 ml. The time for one step that is needed to get a flow rate of $0.1 \mu l/min$ with a 1 ml syringe pump is given in equation 4.14. The syringe pump advances a distance $l_{step} = 0.165 \text{ micron/step}$.

$$\text{Syringe pump : } l_{step} = 0.165 \frac{\text{micron}}{\text{step}}$$

$$1 \text{ ml Hamilton syringe : } \varnothing = 4.61 \text{ mm}$$

$$\begin{aligned}
r &= 0.1 \frac{\mu l}{min} \\
v &= r \cdot \frac{1}{\left(\frac{\varnothing}{2}\right)^2 \pi 60 \frac{s}{min} 1000 \frac{l}{m^3}} \\
&= 0.1 \cdot 10^{-6} \frac{l}{min} \cdot \frac{1}{(0.002305 m)^2 \pi 60 \frac{s}{min} 1000 \frac{l}{m^3}} \\
&= 9.9852 \cdot 10^{-8} \frac{m}{s} \\
t_{step} &= 0.165 \cdot 10^{-6} \frac{m}{step} \cdot \frac{1}{9.9852 \cdot 10^{-8} \frac{m}{s}} = 1.6524 \frac{s}{step}
\end{aligned} \tag{4.14}$$

\varnothing is the diameter of the syringe, r is the flow rate, v is the mean velocity of the syringe pump and t_{step} is the time between two steps. That means that for a flow rate of $0.1 \mu l/min$ the time between two steps is about 1.65 s. So the single steps of the pump will not be noticed in the channel because of the length and expansibility of the tube. This is valid too for flow rates of about $0.025 \mu l/min$ that are needed for the sample flow as stated before.

4.3.2 Particle separation

After the evaluation of the designs given in figure 4.6 only the design presented in this work has been realized. The concept of that separation principle is discussed in chapter 3 in detail.

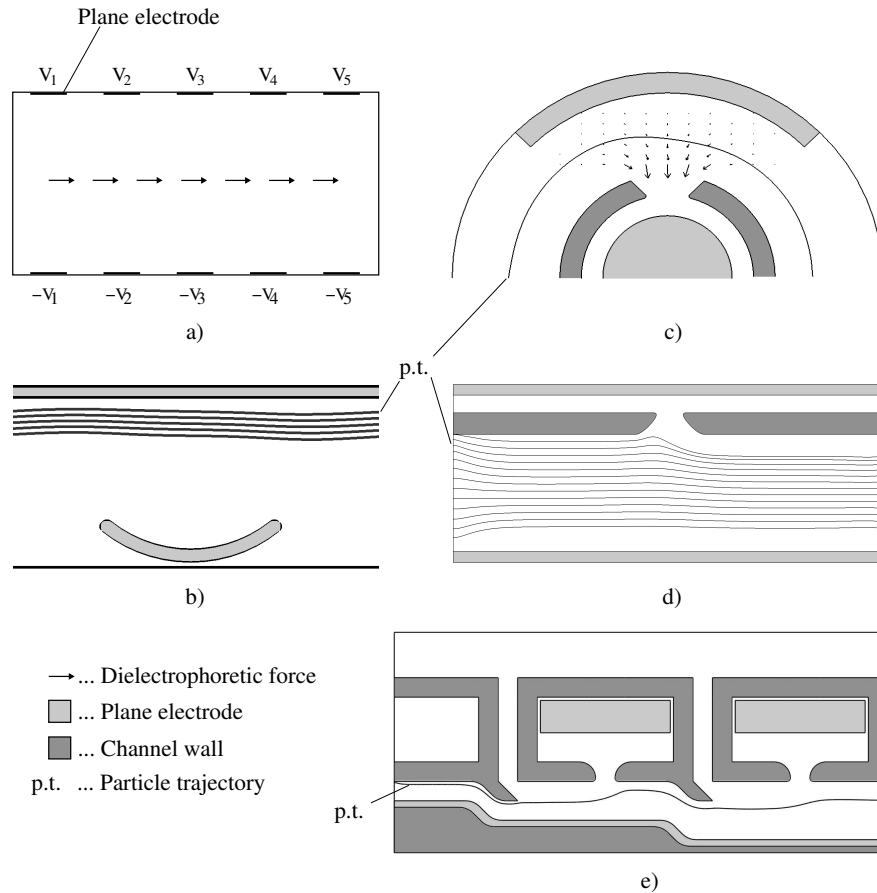


Figure 4.6: Several separation principles that were inspected but not realized because of the mentioned reasons:

a) An isomotive dielectrophoretic force field is produced in the plane of symmetry between the electrodes which are suited on the top and bottom of the channel. This principle is described in [Li and Kaler, 2002]. The DEP force acts perpendicular to the direction of the fluid flow. That design has not been realized because electrodes on top *and* bottom are needed and each electrode needs another voltage. b) The DEP force field of two concentric spheres should have been imitated with this principle. It has not been realized because the particles are likely to be trapped at the edges and the electrodes actually implemented show a higher efficiency. c) The second principle based on the DEP force field of two concentric spheres. The problems arise at the electrode edges and the fluidics of curved channels are hard to handle. d) The main idea was to attract particles with positive dielectrophoresis to the break through in the wall by insulator based DEP force field creation and to avoid trapping by flushing the particles away from the DEP force field peaks using fluid flowing from the narrow to the wide channel. The main problem is the fluid mechanics near the wall openings. e) A very complex principle that is intended to hold off the particles from the break through in the channel wall where the DEP force maxima occur. Here the fluidics are very hard to handle.

Additionally for high conducting suspension fluids the idea arose to insulate the electrodes. The disadvantage of this was that then the electric field mainly drops in the insulation layer since the fluid seems to be a domain of constant potential, like a metal body. Therefore a high-resistance suspension is used, namely 0.4M mannitol.

4.3.3 Evaluation of separation process and sample outlet

To evaluate the separation efficiency a detection area is integrated into the device. Its main purpose is to assist in the optical detection of the particle position and hence the determination of the particle deviation. The principle is shown in figure 4.7. The separation channel is widened about two times, depending on the separation channel width. The width of the detection channel is the same for all design variations that will be introduced in section 4.4.2.

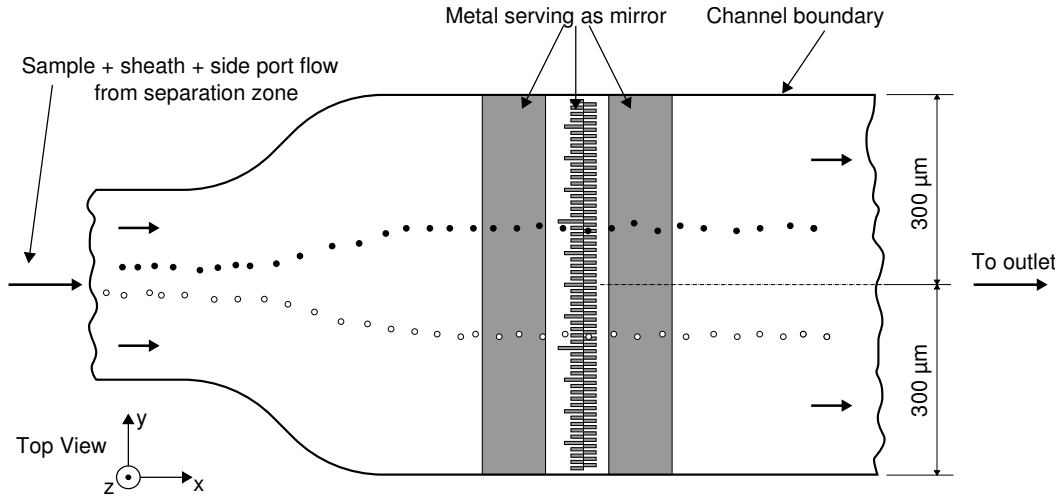


Figure 4.7: Detection area for determination of particle deviation. The total width is $600 \mu m$. The two broad metal mirrors left and right of the scale metal surfaces were added to improve the visibility of the particles in case of bad contrast between particles and substrate. Measurements showed that these two mirrors are not necessary. The scale division is $5 \mu m$, so the left hand side of the scale denotes the positions $[-290, -280, \dots -10, 0, 10, \dots 280, 290] \mu m$, the right hand side the positions $[-285, -275, \dots -5, 5, \dots 275, 285] \mu m$, if a deviation relative from the channel center is considered. So a deviation of $2.5 \mu m$ is detectable for the separation zone for a channel width ratio of 1 : 2 between separation and detection zone.

4.4 Design considerations

In this section the considerations for the design process are presented. The optimization task delivers the optimal electrode geometry for a specific separation channel width, but first that width has to be specified. Additionally the length of the channel depends on the maximum device size and the distances between the inlets. Most of these basic conditions were predetermined by existing hardware, e. g. the device holder.

4.4.1 Requirements

The basic design requirements are

- the position of the inlets since an existing device holder is used presented in section 5.1.1. The minimum distance between the inlets is additionally restricted by the diameter of the o-rings that seal the connection between the tube and the device. There would have been no benefit from designing a new holder since the possible reduction of the distance between the inlets is minimal and an enlargement of the device would have been counterproductive because a certain number of devices has to be placed onto the wafer to increase the distribution of risk of defective devices.
- the placement of the electrodes only on the bottom of the device to ease the production process. Electrodes on the covering glass would have led to a more complicated process.
- the maximum available voltage. The signal generator only provides voltages with a maximum amplitude of $U_P = 10\text{ V}$ for high impedance loads. To widen the separation zone an amplifier was designed that provides a non-inverted and an inverted signal with an amplitude of $U_P = 13\text{ V}$ even for low impedances. The electrodes are connected to the non-inverted and the inverted signal and a resulting peak voltage of $U_P = 26\text{ V}$ is provided, see section 5.1.2.
- the minimum realizable fluid flow speeds. As stated in section 4.3.1 the flow speeds have a lower limit that is about $0.025\text{ }\mu\text{l}/\text{min}$.

These requirements are taken into account in the next section.

4.4.2 Channel dimensions of the design variations

Several variations of the channel geometry were realized. The following considerations were taken into account:

- The shorter the separation channel is the lower the fluid flow speed has to be and vice versa. Therefore a longer separation channel is preferred to avoid the problems with low flow speeds mentioned in section 4.3.1.
- The wider the separation channel is the higher the fluid flow rate can be and vice versa because if the cross section area increases the fluid flow speed stays the same if the fluid flow rate is increased.
- The wider the separation channel is the worse gets the particle focusing if the particles are not exactly aligned in a row in the narrow section of the focusing part.
- The wider the separation channel is the higher the voltage has to be that is applied to the electrodes if they are scaled as well. On the other hand the possible separation zone is wider that leads to larger deviations and less requirements for the particle focusing quality.

- In the separation zone the isosurface planes of the electric voltage have to be perpendicular to the channel top and bottom, therefore the distance from the electrodes to the separation zone has to be larger than the channel height.

The diameter d of the largest cells in the channel are considered to be about $5 \mu m$. Therefore two widths of the separation zone with $50 \mu m$ and $100 \mu m$ were chosen. $50 \mu m$ for a total deviation range of $10 \cdot d$ and $100 \mu m$ for a deviation of $10 \cdot d$ on either side, if the particle starts at the center of the channel. The distance between the separation zone and the electrodes is $50 \mu m$, just enough for the isosurface planes of the electric field to get into a perpendicular orientation to the glass and substrate boundaries. Additionally the channel height has to be smaller than that distance, so it was chosen to be $30 \mu m$.

The four main design variations that were realized consist of a short and a long version for the separation channel and a $250 \mu m$ and $300 \mu m$ wide version for each of them. The device geometries for the short and long version are shown in figure 4.8. The device geometries are summarized in table 4.6.

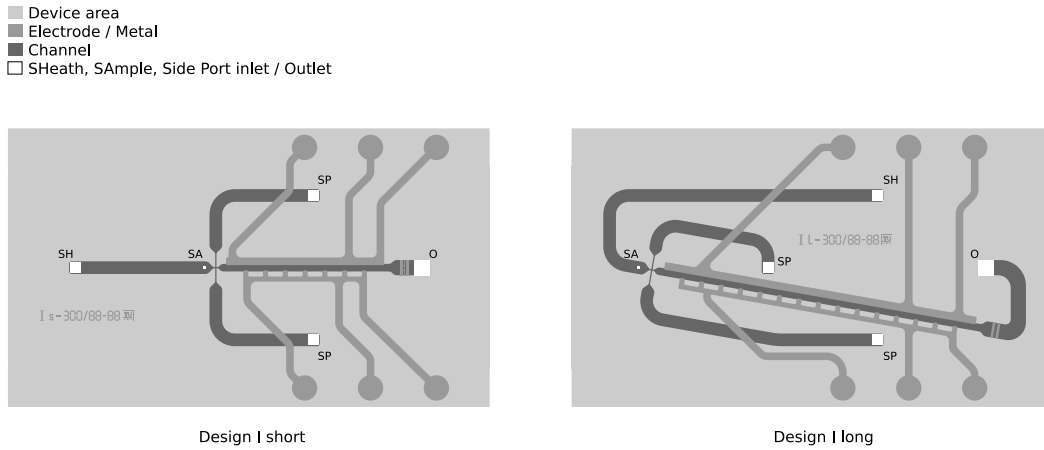


Figure 4.8: For each of this two design variations a version with a $250 \mu m$ and $300 \mu m$ wide separation channel has been realized. The channel in the long version has been rotated slightly to make more use of the device area. The round electrode pads are used to make an electrical connection to the printed circuit board presented in section 5.1.3.

The width of the detection channel is the same for all design variations.

4.5 Materials and fabrication process

For the base material of the device a silicon wafer is used because the inlets and outlets can easily be etched into the substrate in contrast to the drilling necessary for glass as a base material. The wafer is pre-coated on both sides with $250 \text{ nm } SiO_2$ and $70 \text{ nm } Si_3N_4$. As electrode material platinum is used because of its corrosion resistance. The channel itself is formed by the photoresist SU-8 whose thickness can be predetermined with an accuracy of about $1 - 2 \mu m$ with the applied technique of spin coating ([Svasek et al., 2003]). For the

Geometry parameter	Design I short	Des. I short	Des. I long	Des. I long
Separation channel width	250 μm	300 μm	250 μm	300 μm
Separation zone width	50 μm	100 μm	50 μm	100 μm
Separation channel length	5.85 mm	5.46 mm	11.7 mm	11.7 mm
Single DEP unit length	650 μm	780 μm	650 μm	780 μm
Width of small electrode	160 μm	200 μm	160 μm	200 μm
Label on-chip	Is-250/xx-xx	Is-300/xx-xx	Il-250/xx-xx	Il-300/xx-xx

Table 4.6: Geometry of the realized device variations. The text in the last row is printed on the device to distinguish the different versions after fabrication more easily. The part xx-xx is replaced by a row-column numbering to indicate the position on the wafer.

fabrication of the device five masks were drawn in AutoCAD 2004, see appendix B. The process itself is outlined in figure 4.9.

The following steps are taken during the fabrication process:

- Structuring of the SU-8 photoresist with a thickness of 26 μm on the glass wafer that serves as the channel wall. The glass has a thickness of 500 μm :
 - a) Spin coating of SU-8 photoresist onto the glass wafer and exposure of the SU-8 walls to an ultraviolet light source.
 - b) Post exposure bake (PEB) to harden the exposed SU-8.
 - c) Coating of the SU-8 layer with a copper layer (1 μm) that is structured afterwards. That layer protects the hard SU-8 walls and the parts that will be wafer bonded with the silicon wafer.
 - d) The unprotected parts of the SU-8 layer are developed and the protecting copper layer is removed.
- For the devices with an additional insulating SiN_x layer the silicon wafer has to be coated with a nitride layer with a thickness of 800 nm . Then the following steps are taken that are the same for devices without additional insulating layer:
 - e) The electrodes are structured on the silicon wafer with platinum and titanium as undercoating utilizing a lift off process.
 - f) On the bottom of the silicon wafer the existing Si_3N_4 layer is structured that resists the following etching process with KOH.
 - g) Because of the structure of the silicon the angle between the pyramidal hole and the wafer surface is well defined. At the Si_3N_4 layer on the top of the wafer the etching process stops and a thin nitride membraner remains that acts as a basis for the following SU-8 spin coating.
 - h) A 4 μm thick SU-8 layer is spin-coated onto the top of the wafer covering the whole surface including the electrodes and holes.
 - i) Then the SU-8 layer is processed with the same steps that were taken for the glass wafer to structure the hard SU-8 walls and microfluidic channels. That thin SU-8

layer is needed for the wafer bonding process in which the soft parts of the SU-8 layers between the channel walls band together. The nitride layer is removed and the holes are uncovered.

- j) Now the glass and the silicon wafer have to be bonded together. First the two wafers are adjusted and then they are wafer bonded at high pressure and a temperature of 180°.
- Then the resulting wafer has to be sawed in two steps. First the glass wafer is cut between the electrode pads and the microfluidic channels to uncover the electric contacts. In a final step the devices themselves are separated by sawing through the glass and the silicon wafer at the device boundaries.

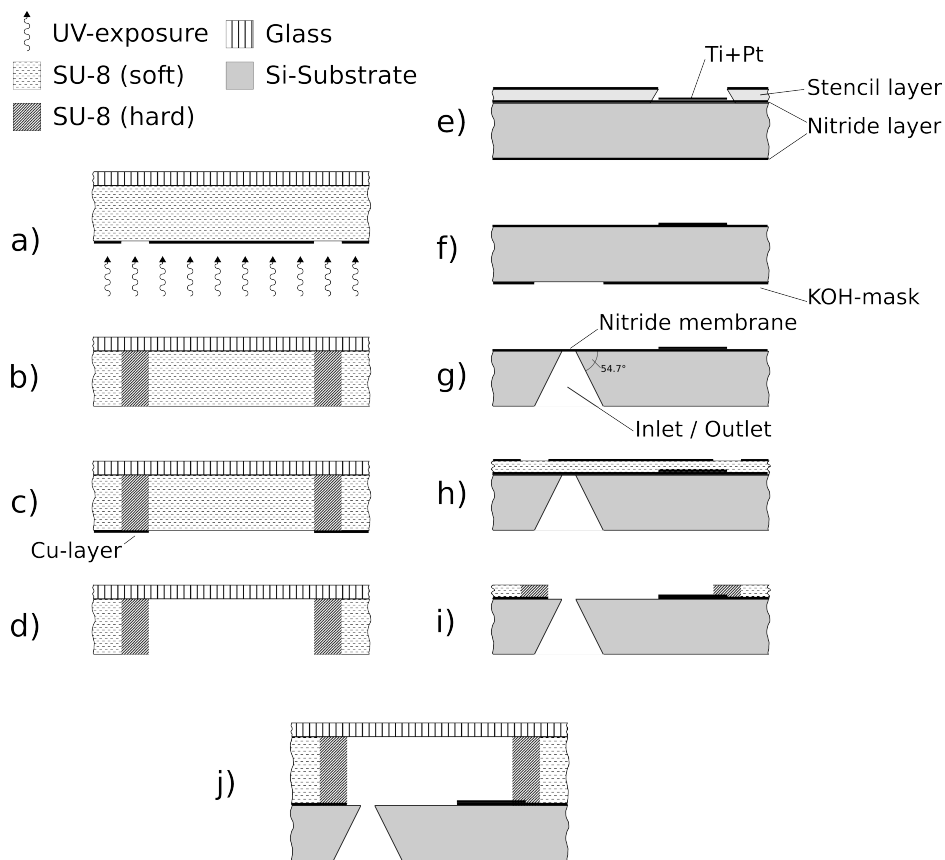


Figure 4.9: Schematic of the device fabrication process. After processing the glass and silicon wafer each on its own they are wafer bonded together. In a final sawing process the devices are then separated.

The fabricated device *Design I* long 300 μm is shown in figure 4.10.

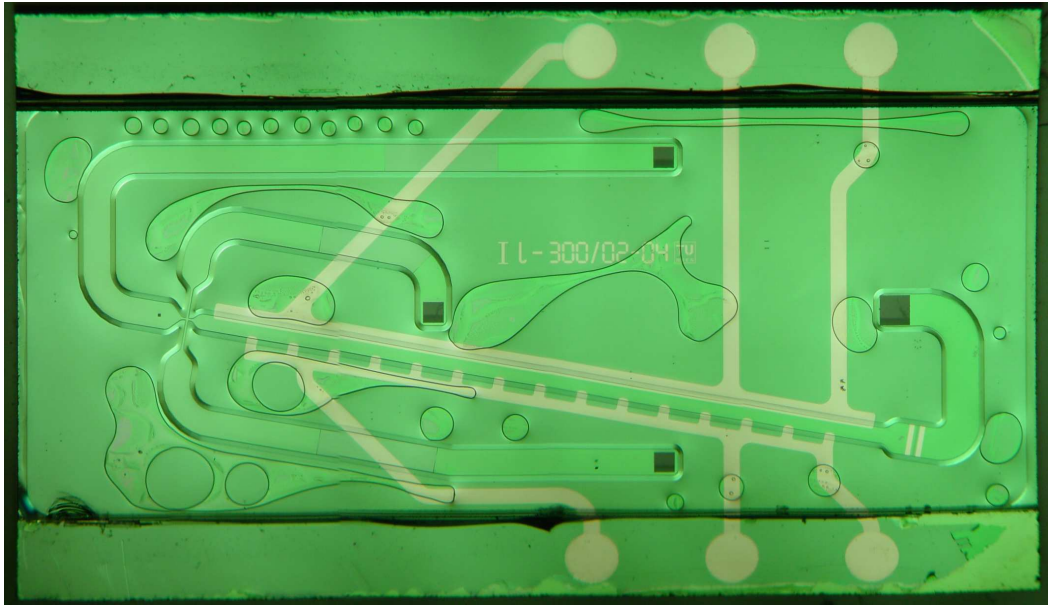


Figure 4.10: Photograph of the fabricated device *Design I long 300 μm* with a size of $11 \times 19 \text{ mm}^2$

5 Measurements

The functional evaluation of the fabricated device is described in this chapter. That includes the experimental setup in chapter 5.1, the measurement work flow in chapter 5.2 and the measurement results together with their interpretation in the chapters 5.3 and 5.4.

The main purpose of the first two chapters is to keep hold of the methods developed and the experience gained during the measurement process.

5.1 Experimental setup

In figure 5.1 the schematic of the entire experimental setup is shown. The device is glued onto a printed circuit board (PCB) that contains the necessary contacts to connect the electrodes with the voltage supply. The PCB is attached to the device holder with four screws which press the device onto the o-rings that seal the connection between the tubes and the in- and outlets of the device, see figure 4.4. The sample, sheath and side port fluids are injected into the device via the tube by four syringes operated by syringe pumps. In figure 5.11 at the end of this chapter a photograph of the experimental setup is shown.

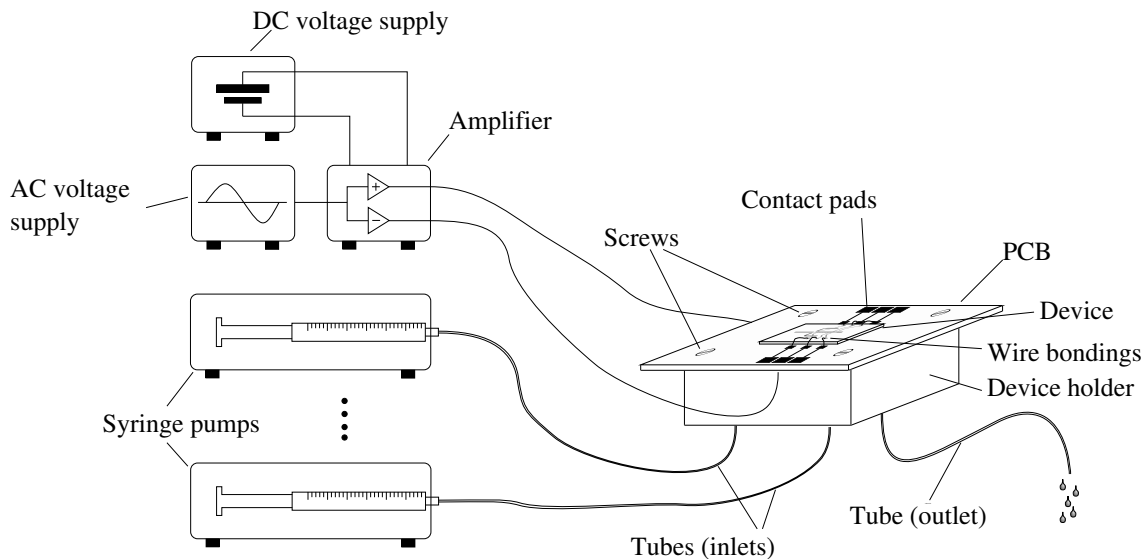


Figure 5.1: The four syringe pumps inject the sample, sheath and side port flows into the device from the bottom through the tubes that are sealed with the device by o-rings (see figure 4.4). The device is mounted on a printed circuit board that is wire bonded to the electrode pads with a copper wire.

Table 5.1 summarizes the equipment that was used for the measurements.

Instrument	Model
Syringe pumps	KD Scientific, Model 200P
Syringes	Hamilton Co., Gastight [®] 1001, 1ml
Stereo microscope	Zeiss Stemi SV11 Apo
Digital camera	Sony Cybershot DSC-S75
Voltage supply (amplifier)	Agilent E3620A
Frequency generator	Hewlett Packard 33120A
Oscilloscope	Tektronix TDS220
Light source	Schott KL 1500 LCD
Network analyzer	Hewlett Packard 8753E
Viscometer	Brookfield DV-II+

Table 5.1: Used equipment for the measurements.

5.1.1 Device holder

The device geometries were adapted to an existing device holder shown in figure 5.2. The holder was fabricated in-house and is made of DELRIN. Previous versions of the device holder needed a plexiglass cover to fixate the chip that was difficult to handle. For the improved design that was used in this work the chip is glued onto a printed circuit board that is screwed onto the device holder. A further advantage of the PCB is that it eases the wire bonding task.

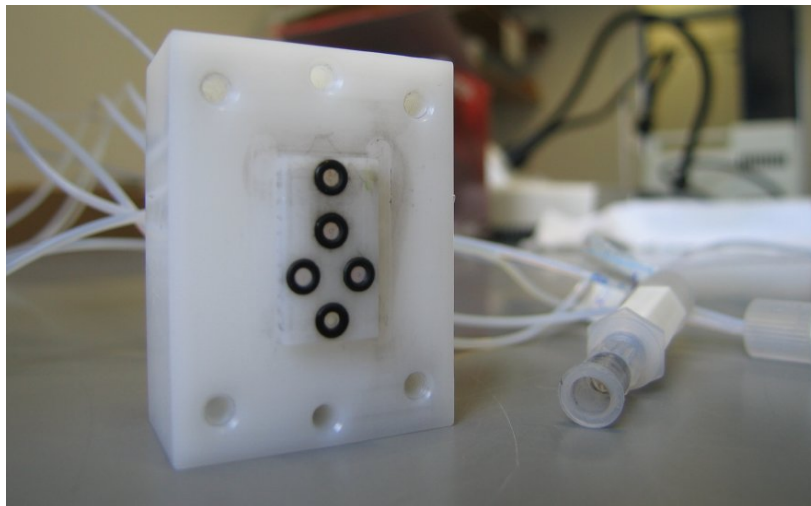


Figure 5.2: The device holder with the screw holes, inlets and outlets with sealing o-rings and the tubes that are connected with the syringes during the experiment.

5.1.2 Voltage supply

Since the maximum voltage for powering the electrodes can not be produced by the frequency generator an external voltage amplifier had to be designed. It consists of a non-inverting and an inverting operational amplifier circuit that amplifies the voltage supplied by the frequency generator by a factor of 4. The schematic of the voltage amplifier is shown in figure 5.3

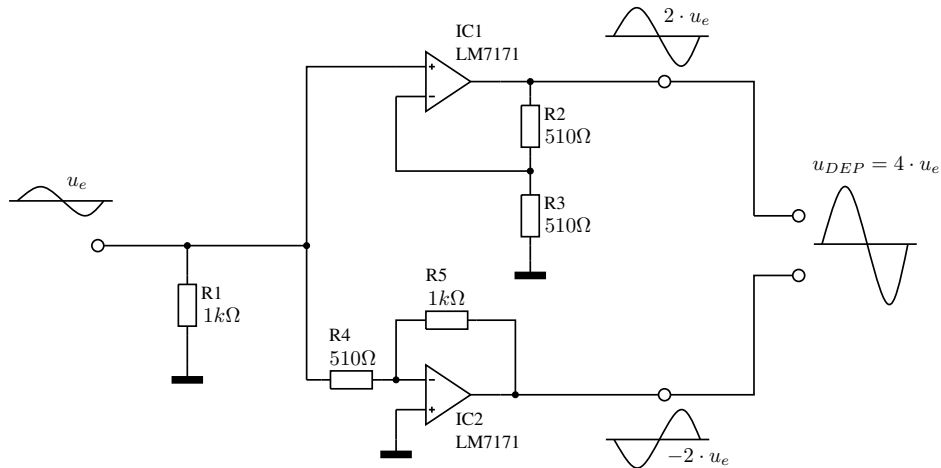


Figure 5.3: The schematic of the voltage amplifier that generates the AC voltage for the DEP electrodes. The signal of the function generator is amplified by a factor of 2 by the non-inverting and inverting operational amplifiers. These two outputs are connected to the two electrodes that produce the electric field in the channel. The resulting DEP voltage at the electrodes is sinusoidal and has a peak voltage of $\hat{U}_{DEP} = 4 \cdot \hat{U}_e$.

5.1.3 Printed circuit board for device bonding

The chip is glued onto a printed circuit board (PCB) that has the following functions:

- Fixation of the microfluidic device on the device holder
- Connection to the voltage supply
- Easy wire bonding of the electrodes on the device

The layout of the board was created with the *EAGLE Layout Editor* and fabricated in-house. Since the wire bonding was done manually with copper wires that were soldered onto the PCB and connected with the device using conductive silver the PCB tracks had not to be gold plated that would have been necessary for ordinary wire bonding. The PCB with an affixed device and the wire bondings is shown in figure 5.4

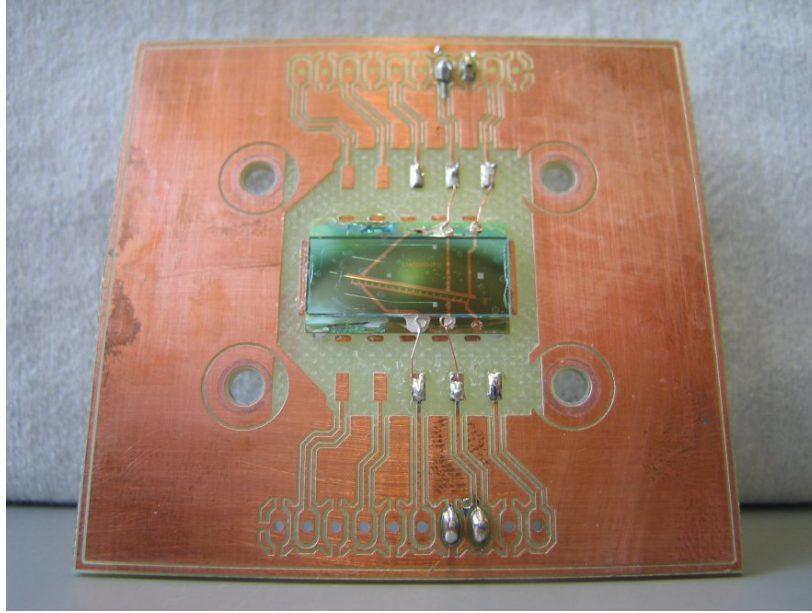


Figure 5.4: The printed circuit board that holds the device and is used to contact the electrode pads. After the contacting the PCB is screwed onto the device holder.

5.2 Measurement work flow

In this section the experience gained during the device measurements are summarized to ease future experimental setups. An extended description of the workflow can be found in appendix C

First the device has to be fixated on the printed circuit board with *Loctite Super Glue*. Then the electrodes are wire bonded with the pads on the PCB using a thin copper wire, applying solder on the PCB and liquid conductive silver on the electrode pads, see Figure 5.5.

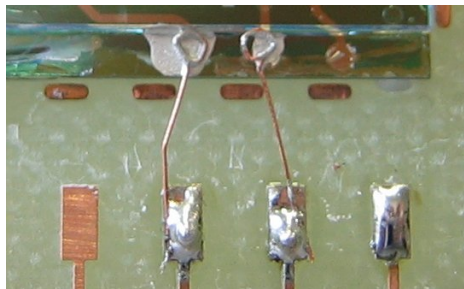


Figure 5.5: The bond pads on the PCB are connected to the electrode pads on the device by soldering thin copper wires onto the PCB and contacting the device with conductive silver.

After the device is glued onto the PCB and the electrode pads are wire bonded the chip is flooded with the desired fluid used for the measurements, e.g. deionized water or mannitol solution, and the bubbles are removed by applying higher flow rates of about $30 \mu m$. Then the device is removed from the device holder and the inlets are covered with small drops of suspension liquid to avoid drying. The device holder is cleaned and the o-rings are flooded with the liquid. After mounting the PCB containing the device with the screws the contact pins on the PCB are connected to the voltage supply. Now the syringe pumps can be turned on with the desired flow rates to start the measurements.

5.2.1 Detection of the particle position

As soon as the beads or cells were centered in the middle of the detection zone, see figure 4.7, a movie was recorded with the digital camera to ease the measurement of the particle deviations. Since the resolution was only 320×240 pixels the metal scale in the detection zone could not be used to determine the particle positions. Therefore an additional scale was overlaid in a post-processing task that was aligned using the larger markings of the original metal scale. Figure 5.6 shows a snapshot of a movie with the additional scale and a particle that crosses the scale at a y-position of about $25 \mu m$.

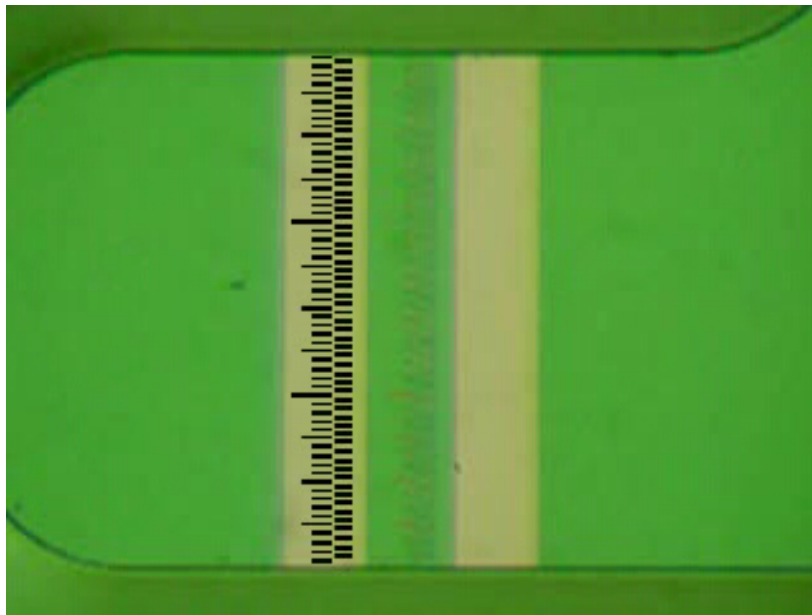


Figure 5.6: Screenshot of a particle crossing the overlaid scale in the detection zone at $25 \mu m$.

For the measurement results presented in the next section the zero position for the particle deviation is in the middle of the channel, see figure 5.7. Particles that are attracted to the smaller electrodes experience positive dielectrophoretic force and move in negative y-direction. Particles that experience negative dielectrophoretic force are repelled from the

smaller electrodes and are moved in positive y-direction.

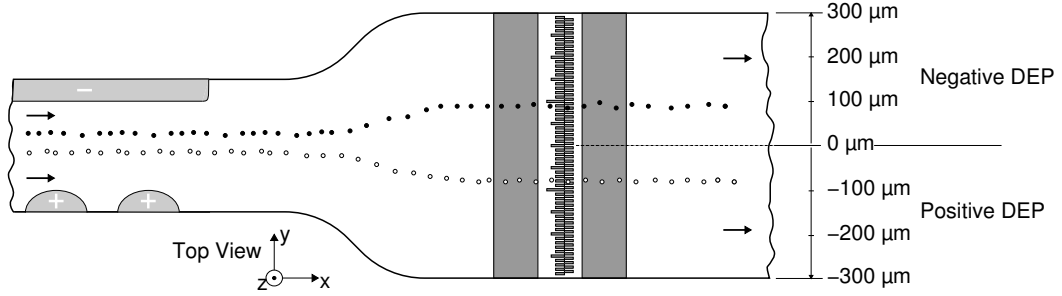


Figure 5.7: Particles that experience positive dielectrophoretic force move in negative y-direction (white particles) and vice versa (black particles).

5.3 Measurement results

The measurement results presented in this section were obtained by recording movies of yeast cells (*Saccharomyces cerevisiae*) and polystyrene beads entering the detection zone with and without applied voltage. To proof the function of the device the deviation of cells and beads was first measured separately. Table 5.2 summarizes the measurement parameters for the following results.

Parameter	Value	Unit	Comment
U_{eff}	11.31	V	Voltage applied to the electrodes
f	1	kHz	Frequency of U applied to the electrodes
U_{DC}	15	V	Supply voltage for the amplifier
v_{sa}	0.05	$\mu l/min$	Sample flow rate
v_{sh}	0.35	$\mu l/min$	Sheath flow rate
v_{sp}	0.4	$\mu l/min$	Side port flow rate
Suspension medium	Mannitol		

Table 5.2: Experimental parameters that led to the presented measurement result.

As the simulation for the Clausius Mossotti factor predicts the yeast cells experienced positive dielectrophoretic force. The Clausius Mossotti factor for the beads was expected to be about $K = -0.48$ that accords to the behavior seen in the separation process.

Figure 5.8 shows the relative frequency distribution of the particle count for yeast cells in the detection zone. It is obvious that the distribution for the yeast cells is moved to the left which means that they experience positive dielectrophoretic force. Additionally the distribution is broadened because of the differing radius of the yeast cells which ranges from $1.5 - 3 \mu m$ and cell division that takes place in the sample. The mean value for the yeast cell positions without voltage is $-1.58 \mu m$ which is shifted to a mean value of $-41.47 \mu m$ if the voltage is applied to the electrodes.

Since the beads have an almost constant radius of $4 \mu m$ the shift of the relative frequency distribution is more clearly to see than for the yeast cells as shown in figure 5.9. The mean value for the particle positions changes from $5.76 \mu m$ to $40.61 \mu m$ if the voltage is applied.

Information about the number of counted particles and statistical data gives table 5.3. A deviation that is less than zero accords to positive DEP, a deviation that is greater than zero means negative DEP.

Parameter	$U_{eff} = 0V$		$U_{eff} = 11.31V$		Units
	Yeast	micromer [®] beads	Yeast	micromer [®] beads	
n	130	152	68	325	
\bar{y}	-1.58	5.76	-41.47	40.61	μm
<i>deviation</i>			-39.89	34.85	μm

Table 5.3: Measurement result parameters. U_{eff} is the effective voltage applied to the electrodes, n is the particle count, and \bar{y} is the mean value for the y-position of the measured particles.

Additionally a mixture of yeast cells and beads was injected into the device to measure the resulting distribution and to show that the separation process works well. Figure 5.10 shows the first results. The distribution looks like a superposition of figures 5.8 and 5.9 and indicates the function of the separation.

5.4 Interpretation

The presented results prove the function of the device. The mean deviations shown in table 5.3 were additionally fitted to the simulation results. Apparently a higher voltage is needed for the real device than in the simulation. A particle distribution comparable to the measured one assumes according to the simulation an effective voltage of about $U_{eff} = 6.5 V$. So the needed voltage is about 74 % higher than the simulated one. The reasons may be:

- The simulation is 2D only, so it is assumed that the electrodes are massive ones ranging over the whole channel height. In the real device the electrodes are plane electrodes. That behavior has been considered and confirmed during the simulation process.
- The viscosity of the fluid affects the separation process heavily and it can not be determined exactly. So it may be higher than the measured value shown in table 4.5 and a higher force and therefore a higher voltage is needed to move the particles..

The simulated deviation for the yeast cells and the beads is almost the same but in different directions. That conforms to the measurement result. Although the beads have a larger diameter their Clausius Mossotti factor is smaller than that of the yeast cells and additionally the DEP force decreases if the beads are moved away from the smaller electrodes. That explains why the deviations of this two particle types is nearly the same.

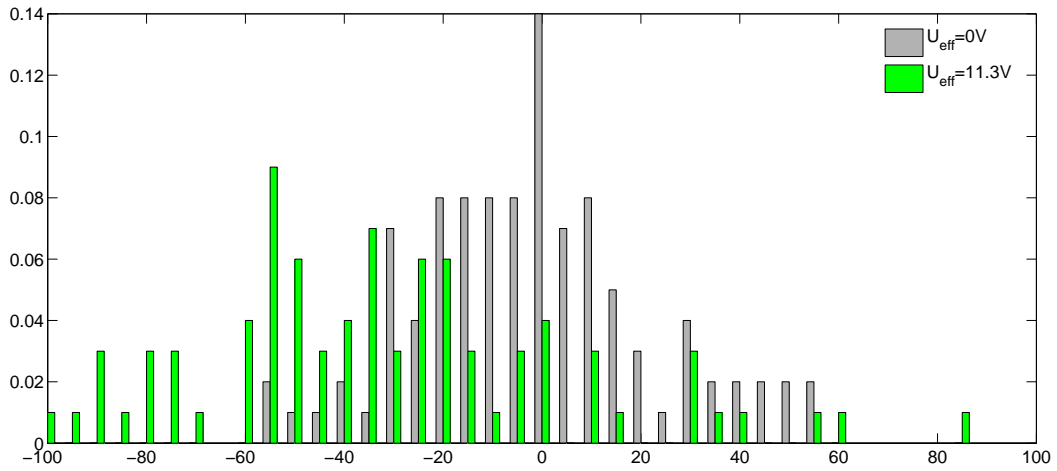


Figure 5.8: The particle deviation for yeast cells (*Saccharomyces cerevisiae*) with a radius of about $1.5 - 3 \mu m$. The gray bars mark the particle count without dielectrophoretic force applied. The maximum particle count is at $0 \mu m$, with the point of origin in the middle of the channel. When an effective voltage of $11.31 V$ is applied the maximum particle count of the particle distribution moves to a deviation of $-55 \mu m$ with a mean value of $-41.47 \mu m$. The particles were counted at intervals of $5 \mu m$ in y -direction.

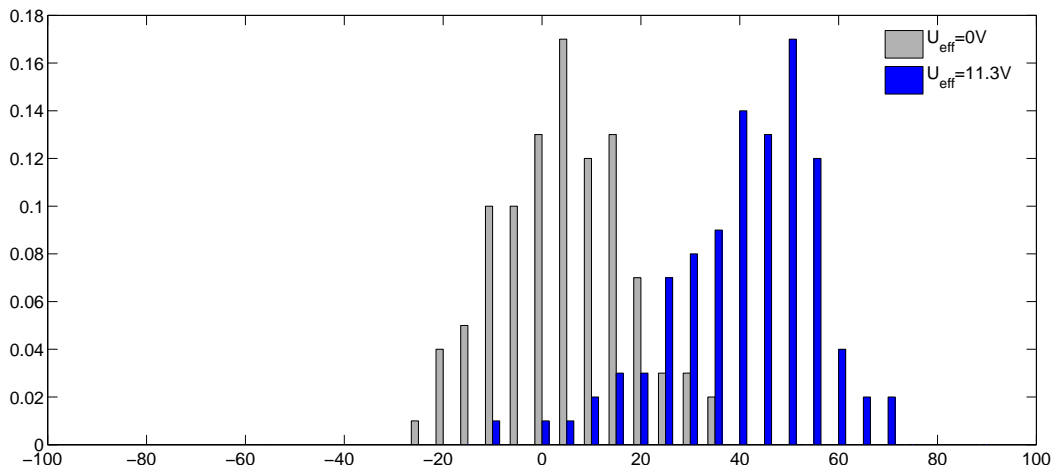


Figure 5.9: The particle deviation for micromer[®] beads with a radius of $4 \mu m$. The gray bars mark the particle count without dielectrophoretic force applied. The maximum particle count is at $5 \mu m$, with the point of origin in the middle of the channel. When a effective voltage of $11.31 V$ is applied the center of the particle distribution is at a deviation of $50 \mu m$. The particles were counted at intervals of $5 \mu m$ in y -direction.

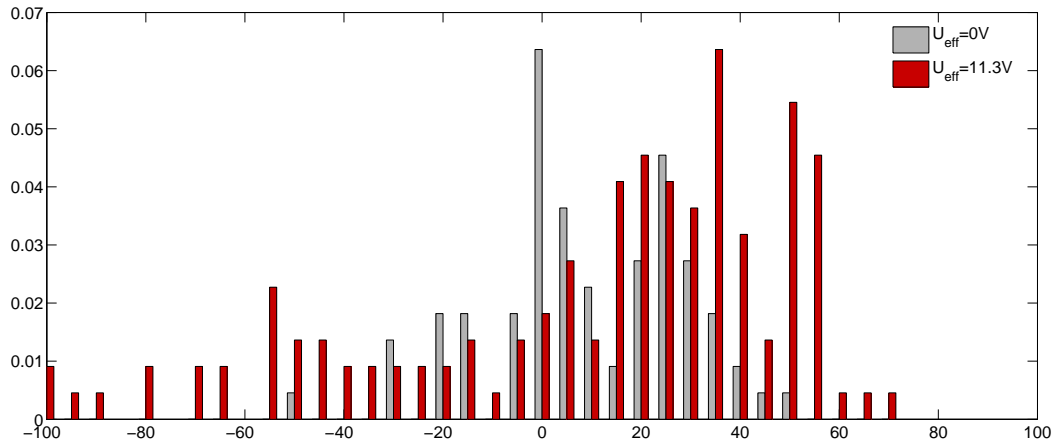


Figure 5.10: The relative frequency distribution of the particle count for a mixture of yeast cells and beads. The gray bars denote the distribution without applied voltage whereas the red bars show the distribution for an applied voltage of $U_{eff} = 11.31 \text{ V}$. The particles were counted at intervals of $5 \mu\text{m}$ in y -direction.



Figure 5.11: Photograph of the experimental setup. On the left are three syringe pumps placed, in the center can the stereo microscope and the device holder with the mounted PCB and device be seen and on the right are the amplifier, the power sources and the oscilloscope.

6 Discussion

In this chapter the separation process will be evaluated and several improvements are discussed. It is hardly possible to consider all physical effects that take effect in a complex device as the one presented in this work so the actual behavior of the system leads to conclusions for an optimization of the design.

The following potential issues that may arise in the realized design have been considered:

1. The joule heating in the fluid due to its conductivity. Therefore a saline solution like 0.9% *NaCl* as suspension medium was unsuitable. So a 0.4M *mannit* solution was used that has a higher conductivity than deionized water but a lower conductivity than saline solution.
2. The influence of the silicon substrate as a consequence of the electric field coupling into the silicon substrate has been expected to become critical at frequencies higher than 30 *kHz*. On the one hand the current through the substrate increases the load acting on the voltage amplifier, on the other hand the potential in the substrate couples back into the separation channel and affects the electric field negatively.
3. Electrode erosion is minimized by using a low conducting suspension medium like mannit solution. Experiments showed that applying the highest possible voltage of $U_{eff} = 19.5 V$ even at low frequencies of $f = 1 kHz$ did not lead to any noticeable electrode erosion process.
4. The size of the sample inlet and the width of the focusing unit were designed for particles with a radius of about 2 – 4 μm based on existing devices. A smaller sample inlet does not lead necessarily to a narrower particle distribution in the separation zone because at the same sample flow rate the pressure at the inlet in the channel increases and the inflow is broadened. Additionally smaller inlets increase the risk of particle clogging. It was expected that the yeast cells can be focused with an absolute deviation of 5 μm in each horizontal direction.
5. The viability of the yeast cells heavily depends on the osmolarity of the suspension medium, therefore deionized water could not be used. Due to the demand for a medium with low conductivity a 0.4M *mannit* solution was used which was tested for its suitability with a viability test.

Based on the actual function of the device the following conclusions about the correctness of the considerations shown above can be made:

1. Since the fluid did not show any remarks of heating at high voltages and low frequencies, where the influence of silicon substrate heating can be neglected, this assumption can be considered as correct.

2. The influence of the conductivity of the silicon substrate on the function of the device is obviously more problematic as expected. Turbulences in the fluid due to heating of the medium were observed even at frequencies lower than 30 kHz . The reason might not be the joule heating in the fluid itself but rather the heating at the electrode edges due to the current through the substrate. So a very low frequency of 1 kHz was used for the experiments at which these turbulences were not present.
3. Electrode erosion was not visible both with a test device without channel geometries and the actual device with channel geometries.
4. The focusing of the particles was found to be difficult. With the applied flow rates the minimum absolute deviation of the particles in the separation zone was about $10\text{ }\mu\text{m}$.
5. The yeast cells experienced a positive dielectrophoretic force even after 2 hours, so it can be assumed that the viability of the cells did not decrease during that time.

The presented observations lead to the possible improvements discussed in section 6.2.

The original intention to use E.coli bacteria in the experiments was abandoned because organisms of that size would not have been detectable with the stereo microscope and the used camera.

6.1 Separation efficiency

The separation efficiency becomes better with decreasing width of the particle distribution over their y-position and increasing deviation of that distribution, see figure 6.1.

To decrease the width of the particle distribution for the same width of the detection zone it is possible to

- redesign the channel geometries to improve the focusing of the particles or to
- increase the flow rates. That would imply a more smooth fluid stream since the single steps of the syringe pumps would occur more frequently. Another possibility is to
- increase the width of the separation channel so the ratio between the detection channel and the separation channel gets smaller and the particle distribution in the separation channel is less broadened. The disadvantage would be that higher voltages are needed at the electrodes to get a dielectrophoretic effect that leads to the same particle deviation in the detection zone.

To increase the mean deviation of the particles for the same width of the detection zone it is possible to widen the separation zone and apply a higher voltage at the electrodes.

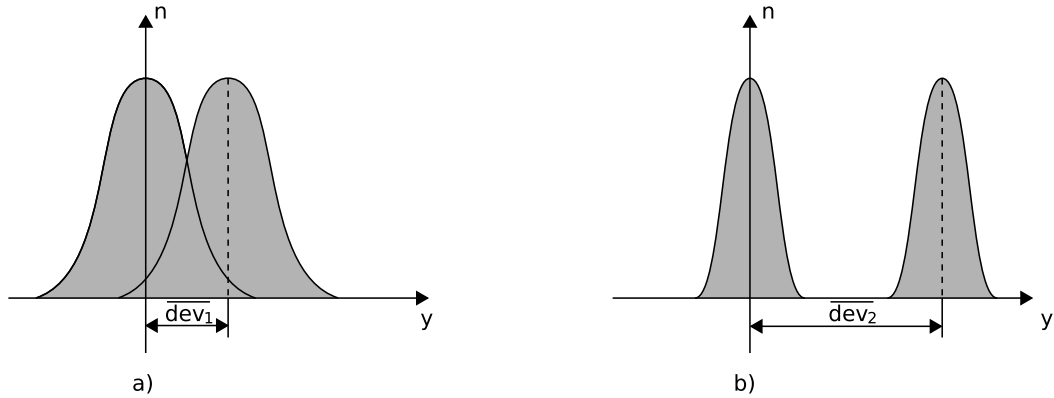


Figure 6.1: The separation shown in (a) is improved if the mean of deviation is increased from \overline{dev}_1 to \overline{dev}_2 and the width of the distribution (grey area) gets smaller. n is the particle count and y denotes the position of the particles in the detection zone.

To benefit from widening the separation zone it is necessary to improve the focusing of the particle because if the separation zone is expanded not only the mean deviation is increased but also the width of the distribution.

6.2 Device improvements

Summarizing the last two sections the most important improvements that can be made to the device presented in this work are

- the improvement of the focusing unit and
- the replacement of the silicon by a glass substrate.

The advantages of an improved particle focusing were discussed in the previous section in detail. It could be realized by decreasing the size of the sample inlet and lowering the flow rate of the sample flow. Another possibility is to reduce the width of the channel in the focusing unit to narrow the sample flow as much as possible. The better the particles are focused in that channel the less they are dispersed when the channel is broadened again [Hang et al., 2005].

If the silicon substrate is replaced by glass the channel structures have to be redesigned because the minimum diameter of the sample inlet is then about $200 \mu m$, in contrast to the one of the realized device with a side length of about $50 \mu m$.

6.3 Outlook

Further measurements are going to take place for the presentation of the developed device at the μTAS conference in october 2007. The abstract for this conference can be found in appendix D. In future designs the improvements mentioned in the last section should be implemented and the following considerations could be taken into account too:

- Design of a new device holder to increase the separation channel length and to use the device area more efficiently.
- Usage of a camera, e.g. a high definition camcorder, with a higher resolution than the one utilized in the presented measurements to make direct use of the metal scale provided in the detection zone.
- The channel can be split-up in two or more branches to realize a real separation of particles. A SU-8 bar in the middle of the channel could be used to separate particles that show positive and negative dielectrophoretic behavior.
- With an additional inlet following the sample flow inlet the latter one can be lifted vertically to position the particles in the middle of the channel where the velocity gradient of the fluid is smaller than at the bottom of the channel. As a result all particles would move with almost the same velocity.

Conclusions

A new device for a separation device based on dielectrophoresis was developed in this work. The whole design process from the basic ideas to the experimental results was presented. The function of the design principle was successfully proved by the separation of yeast cells and polystyrene beads and the separation efficiency was evaluated. The results accord to the simulated and expected behavior.

Possible improvements of the device include a redesign of the sample injection and focusing unit and the replacement of the silicon substrate by a less conducting material, e.g. glass.

A Model implementation in Matlab

inspectDesigns.m

```
clear;

%Simulation settings
cw = 150e-6; %Separation zone plus forbidden zones that should be simulated
timeStep = 0.001;
v_medium.vol = 1.2e-6; %in l/min
v_medium = v_medium.vol/(cw+100e-6)/30e-6/60/1000%; %in m/s
U_electrode = 6.3; %in Volts
eta_medium = 1.03e-3; %in Pa*s

%Testparticles
particle1.r = 2.5e-6; %Radius
particle1.K = 0.7; %Clausius Mossotti factor

particle2.r = 4e-6;
particle2.K = -0.48;

simSetIndex = 0;

%Define the designs and their the channel and electrode geometries for the
%channels that should be simulated.
if cw == 150e-6
    %The optimal designs (cw = 150e-6):

    simSetIndex = simSetIndex + 1;
    index = 0;
    index = index + 1;
    simulationSets(simSetIndex).simulations(index) = getSimulationForDesign (1, cw, 650e-6, 160e-6);
elseif cw == 200e-6
    %The optimal design (cw = 200e-6):

    simSetIndex = simSetIndex + 1;
    index = 0;
    index = index + 1;
    simulationSets(simSetIndex).simulations(index) = getSimulationForDesign (1, cw, 780e-6, 200e-6);
end

%Cut off trajectories if they leave the range denoted with rangeMinMaxY
rangeMinMaxY = [50e-6 cw-50e-6];

testParticleIndex = 0;

%Different start positions for differet channel widths.
%Start in the center of the separation zone
if cw == 150e-6
    testParticleIndex = testParticleIndex + 1;
    testParticle.startPointY = 75e-6;
    testParticle.particle = particle1;
    testParticles(testParticleIndex) = testParticle;

    testParticleIndex = testParticleIndex + 1;
    testParticle.startPointY = 75e-6;
    testParticle.particle = particle2;
    testParticles(testParticleIndex) = testParticle;
elseif cw == 200e-6
    testParticleIndex = testParticleIndex + 1;
    testParticle.startPointY = 100e-6;
    testParticle.particle = particle1;
    testParticles(testParticleIndex) = testParticle;

    testParticleIndex = testParticleIndex + 1;
    testParticle.startPointY = 100e-6;
    testParticle.particle = particle2;
    testParticles(testParticleIndex) = testParticle;
end

%Calculate and plot the optimization visualized in 3D for a channel with a
%width of 250um. The value 150um denotes the width of the separation zone
%plus the two forbidden zones.
```

```

try
    clRange = [500e-6:200e-6:900e-6];
    ewRange = [100e-6:50e-6:200e-6];
    designNr = 1;

    plotOptimizationForDesign (testParticles, designNr, 150e-6, clRange, ewRange, rangeMinMaxY, ...
        v_medium, U_electrode, eta_medium, timeStep, 1, 3e-3);
catch
    msg = lasterr
end

%Plot the trajectories for the two test particles with the optimized values
%for the electrode width and DEP channel length
plotTrajectoriesForWholeChannel (simulationSets, testParticles, rangeMinMaxY, v_medium, U_electrode, ...
    eta_medium, timeStep, 1, 11.7e-3);

```

plotOptimizationForDesign.m

```

function plotOptimizationForDesign (testParticles, designNr, cw, clRange, ewRange, rangeMinMaxY, v_medium, ...
    U_electrode, eta_medium, timeStep, bChannelLength, channelLengthOrCount)

for simSetIndex = 1:1:size(clRange,2)
    for simulationIndex = 1:1:size(ewRange,2)
        simulationSets(simSetIndex).simulations(simulationIndex) = ...
            getSimulationForDesign (designNr, cw, clRange(simSetIndex), ewRange(simulationIndex));
    end
end

simulationSets = calcDeviationsForDesign (simulationSets, testParticles, rangeMinMaxY, v_medium, ...
    U_electrode, eta_medium, timeStep, bChannelLength, channelLengthOrCount);

[xValues, yValues] = meshgrid (ewRange, clRange);

for index = 1:1:size(testParticles, 2)
    deviationsForTestParticles(index).zValues = zeros (size(clRange,2), size(ewRange,2));
end

for simSetIndex = 1:1:size(simulationSets,2)
    simulations = simulationSets(simSetIndex).simulations;

    for simulationIndex = 1:1:size(simulations, 2)
        simulation = simulations(simulationIndex);
        devTestParticles = simulation.testParticles;

        for index = 1:1:size(devTestParticles,2)
            deviationsForTestParticles(index).zValues(simSetIndex, simulationIndex) = devTestParticles(index).deviationForWholeChannel;
        end
    end
end

%Create a 3D plot for each test particle
for index = 1:1:size(testParticles,2)
    figure;
    legend_strs = [];
    hold all;

    zValues = deviationsForTestParticles(index).zValues;
    surf (xValues, yValues, zValues);
    grid off;
    hold off;
    set (gcf, 'Name', ['WholeChannel!', 'Design ' num2str(designNr) ', cw=' num2str(cw) ...
        ', wcl=' num2str(channelLengthOrCount) ', U=' num2str(U_electrode) ...
        ', v=' num2str(v_medium) ', r=' num2str(testParticles(index).particle.r) ...
        ', yStart=' num2str(testParticles(index).startPointY)]);
end

```

getSimulationForDesign.m

```

function simulation = getSimulationForDesign (designNr, cw, cl, ew)

%Generate the file name for restoring and saving the simulated data
name = strcat('Design', num2str(designNr), '%02g', '_cw', num2str(cw, '%20g'));
num = nargin;
clInt = cl;

name = strcat (name, '_c', num2str(cl, '%1.6f'), '_e', num2str(ew, '%1.6f'));

filename = strcat (name, '.mat');

```

```

simDir = 'SimulationData';
fileNameWithPath = [simDir filesep filename];

%does the directory 'SimulationData' exist?
%if not, create it
if (~length(dir(simDir))>0)
    mkdir (simDir);
end

%first check if the simulation has been saved to disk previously
%and if so, load it
if (length(dir(fileNameWithPath))>0)
    data = load (fileNameWithPath);
    fdep0 = data.fdep0;
else
    %otherwise, compute the simulation and save it to a file
    fdep0 = simulateFdep0ForDesign (designNr, cw, clInt, ew);
    save (fileNameWithPath, 'fdep0', '-compress');
end

simulation.name = name;
simulation.fdep0 = fdep0;
simulation.cw = cw;
simulation.cl = clInt;
simulation.ew = ew;
simulation.designNr = designNr;

end

```

simulateFdep0ForDesign.m

```

function fdep0 = simulateFdep0ForDesign (designNr, cw, cl, ew)

%The requested design is simulated ...
fem_sim = simulateDesign (designNr, cw, cl, ew);

%... and then a regular grid with the simulated electric field data is generated
fem_pd.x = posteval (fem_sim, 'Fdep0');
fem_pd.y = posteval (fem_sim, 'Fdepy0');
[XI,YI] = meshgrid(-cl/2:1e-6:cl/2, 0e-6:1e-6:cw);
fdep0.x = -cl/2:1e-6:cl/2;
fdep0.y = 0e-6:1e-6:cw;
fdep0.data = griddata (fem_pd.x.p(1,:), fem_pd.x.p(2,:), fem_pd.x.d, XI, YI);
fdepy0.x = -cl/2:1e-6:cl/2;
fdepy0.y = 0e-6:1e-6:cw;
fdepy0.data = griddata (fem_pd.y.p(1,:), fem_pd.y.p(2,:), fem_pd.y.d, XI, YI);

fdep0 = {fdep0 fdepy0};

end

```

simulateDesign.m

```

function fem = simulateDesign (designNr, cw, channelLength, electrodeWidth)

fclear fem

%Get the geometry and the boundary conditions for the requested design that can be simulated in COMSOL Multiphysics
[g, bnd] = getSimDataForDesign (designNr, cw, channelLength, electrodeWidth);

% Constants
fem.const = {'V.electrode','1', ...
    'v.medium','1e-3', ...
    'rho.medium','1050', ...
    'epsr.medium','80', ...
    'sig.medium','1.5e-2', ...
    'eta.medium','8.9e-4', ...
    'rho.iso','1190', ...
    'epsr.iso','3', ...
    'sig.iso','1e-14', ...
    'r.Y','2.5e-6', ...
    'K.Y','1', ...
    'k1.Y','4*pi*eta.medium*r.Y', ...
    'r.EC','1e-6', ...
    'K.EC','1', ...
    'k1.EC','4*pi*eta.medium*r.EC'};

%g is created by the getSimDataForDesignXX function
clear s

```

```

s.objs={g};
s.name={'CO1'};
s.tags={'g'};

fem.draw=struct('s',s);
fem.geom=geomcsg(fem);

% Initialize mesh
fem.mesh=meshinit(fem);

% Refine mesh
fem.mesh=meshrefine(fem, 'mcase',0, 'rmethod','regular');

% Refine mesh
fem.mesh=meshrefine(fem, 'mcase',0, 'rmethod','regular');

% (Default values are not included)

% Application mode 1
clear appl
appl.mode.class = 'QuasiStatics';
appl.module = 'EM';
appl.assignsuffix = '_emqvw';
clear prop
prop.elemdefault='Lag2';
prop.analysis='smallcurr';
appl.prop = prop;

%bnd is created by the getSimDataForDesignXX function
appl.bnd = bnd;
clear equ
equ.epsilon = 'epsr_medium';
equ.sigma = 'sig_medium';
equ.ind = [1];
appl.equ = equ;
fem.appl{1} = appl;
fem.frame = {'ref'};
fem.border = 1;
fem.units = 'SI';

% Subdomain expressions
clear equ
equ.ind = [1];
equ.dim = {'V'};
equ.expr = {'Fdepx0','2*pi*epsilon0_emqvw*epsr_medium*diff(normE_emqvw^2,x)', ...
            'Fdepy0','2*pi*epsilon0_emqvw*epsr_medium*diff(normE_emqvw^2,y)'};
fem.equ = equ;

% Multiphysics
fem=multiphysics(fem);

% Extend mesh
fem.xmesh=meshextend(fem);

% Solve problem
fem.sol=femlin(fem, 'solcomp',{'V'}, 'outcomp',{'V'});

end

```

getSimDataForDesign.m

```

function [g, bnd] = getSimDataForDesign (designNr, cw, channelLength, electrodeWidth)

    wallWidth = 30e-6; %minimal width of SU8 walls, depends on the channel height

    %Create the COMSOL Multiphysics geometries for the requested design
    if (designNr == 1)
        g2=ellip2(50e-6,50e-6,'base','center','pos',[0,-50e-6]);
        g3=rect2(2.0E-4,1.0E-4,'base','corner','pos',[-1.0E-4,-(1E-4+50e-6)]);
        g4=geomcomp({g2,g3},'ns',{'E1','R2'},'sf',{'E1-R2','edge','none'});
        [g, bnd] = getSimDataForDesignInt (cw, channelLength, electrodeWidth, 100e-6, g4, 3);
    end

end

%Scale the given template design to the requested geometries and set the boundary conditions
function [g, bnd] = getSimDataForDesignInt (cw, ch_length, el_width, ...
    el_template_width, el_template_geom, el_template.bndCnt)
    el_scale = el_width/el_template_width; %scaling factor for the electrode

    % Geometry
    g1=rect2(num2str(ch_length),num2str(cw+50e-6),'base','corner','pos', ...

```

```

        {num2str(-ch.length/2),num2str(-50e-6)},'rot','0');

g2=move(el.template.geom, ch.length/2+el.template.width,0);

draw{1} = g1;
draw{2} = g2;
% Create analyzed geometry
femInt = [];
femInt = geomanalyze(femInt,draw,'ns',{ 'R1', 'CO1' });

% Modify geometry in draw structure
r1 = drawgetobj(femInt,'R1');
co1 = drawgetobj(femInt,'CO1');
co1 = move(co1, -(ch.length/2+el.template.width), 0);
co1 = scale(co1, el.scale, 1);
co2 = geomcomp({r1,co1},'ns',{ 'R1', 'CO1' },'sf','R1-CO1','edge','none');
femInt = drawsetobj(femInt,'R1', co2);

% Re/analyze geometry, and update boundary conditions
[femInt, assocmap] = geomanalyze(femInt);

g = co2;

potentialBnds = find(assocmap{2}>=5);
gndBnds = find(assocmap{2}==3);
isolatorBnds1 = find(assocmap{2}<=2);
isolatorBnds2 = find(assocmap{2}==4);
isoBnds = [isolatorBnds1 isolatorBnds2];
potBnds = potentialBnds(1:size(potentialBnds,2)-el.template.bndCnt);

clear bnd;

bnd.V0 = {0,0,'V.electrode'};
bnd.etype = {'V0','nJO','V'};
bnd.ind = {gndBnds isoBnds potBnds};
end

```

calcDeviationsForDesign.m

```

function simulationSetsRet = calcDeviationsForDesign (simulationSets, testParticles, rangeMinMaxY, ...
    v_medium, U_electrode, eta_medium, timeStep, bChannelLength, channelLengthOrCount)

%First the trajectories are calculated
simulationSetsInt = calcTrajectoriesForWholeChannel (simulationSets, testParticles, rangeMinMaxY, ...
    v_medium, U_electrode, eta_medium, timeStep, bChannelLength, channelLengthOrCount);

for simSetsIndex = 1:1:size(simulationSetsInt, 2)
    simulations = simulationSetsInt(simSetsIndex).simulations;
    for index = 1:1:size(simulations,2)
        simulation = simulationSetsInt(simSetsIndex).simulations(index);

        for testParticleIndex = 1:1:size(simulationSetsInt(simSetsIndex).simulations(index).testParticles, 2)

            [ew, deviation] = getDeviationData (simulation, testParticleIndex, bChannelLength, channelLengthOrCount);

            %store the calculated deviation in the simulationSets structure
            simulationSetsInt(simSetsIndex).simulations(index).testParticles(testParticleIndex).deviationForWholeChannel = deviation;
        end
    end
end

simulationSetsRet = simulationSetsInt;
end

function [ew, deviation] = getDeviationData (simulation, testParticleIndex, bChannelLength, channelLengthOrCount)

%The length can be given as channel length or count of DEP units
if bChannelLength == 1
    trajIndex = channelLengthOrCount * 1e6;
else
    trajIndex = channelLengthOrCount;
end

start = simulation.testParticles(testParticleIndex);

display ([ 'In getDeviationData for designNr=' num2str(simulation.designNr) ', cw=' num2str(simulation.cw) ...
    ', cl=' num2str(simulation.cl) ', ew=' num2str(simulation.ew) ', yStart=' num2str(start.startPointY) ] );

trajectory = start.trajectoryForWholeChannel{trajIndex};

```



```

%channel is much larger than one channel unit the deviation is
%small (e.g.: with a channel unit of 400e-6 only a whole channel
%length of 4e-3 or 4.4e-3 can be realized, but not a channel length
%of 4.2e-3
if bChannelLength == 1
    calcCount = ceil (channelLengthOrCount / simulation.cl);
else
    calcCount = channelLengthOrCount;
end

rangeMinMaxX = [-(simulation.cl/2-1e-6) simulation.cl/2-1e-6];

for testParticleIndex = 1:size(testParticles, 2)
    trajectory = [0 0];
    startPoint = [-(simulation.cl/2-1e-6) testParticles(testParticleIndex).startPointY];
    particle = testParticles(testParticleIndex).particle;

    if bChannelLength == 1
        trajIndex = channelLengthOrCount * 1e6;
    else
        trajIndex = channelLengthOrCount;
    end

    %if the data has already been calculated skip this step
    try
        if size(simulation.testParticles(testParticleIndex).trajectoryForWholeChannel,2) >= trajIndex
            if size(simulation.testParticles(testParticleIndex).trajectoryForWholeChannel{trajIndex}, 2) == 2
                continue;
            end
        end
    catch
        %calculate the trajectories
    end

    for calcIndex = 1:1:calcCount
        actTrajectory = calcTrajectory (particle, startPoint, rangeMinMaxX, rangeMinMaxY, v_medium, ...
            U.electrode, eta_medium, timeStep, 1, '', simulation.fdep0);

        lastTrajectoryIndex = size (trajectory, 1);
        lastActTrajectoryIndex = size (actTrajectory, 1);

        startPoint = [-(simulation.cl/2-1e-6) actTrajectory(lastActTrajectoryIndex, 2)];

        if actTrajectory(1,1) == 0 && actTrajectory(1,2) == 0
            break;
        end

        if trajectory(1,1) == 0 && trajectory(1,2) == 0
            trajectory = actTrajectory;
            continue;
        end

        shiftMatrix = [ones(lastActTrajectoryIndex,1) zeros(lastActTrajectoryIndex,1)];
        shiftMatrix = shiftMatrix*(simulation.cl*(calcIndex-1));
        trajectory = cat (1, trajectory, actTrajectory+shiftMatrix);
    end

    testParticles(testParticleIndex).trajectoryForWholeChannel{trajIndex} = trajectory;
end

simulationSets(simSetsIndex).simulations(index).testParticles = testParticles;

end
end

simulationSetsRet = simulationSets;

end

```

calcTrajectory.m

```

function trajectory = calcTrajectory (particle, startPoint, rangeX, rangeY, v_medium, U_electrode, eta_medium, timeStep, ...
    returnOnlyTrajectoriesInsideChannel, v_field.OR_femstruct, Fdep0_field)

k1 = 6*pi*eta_medium*particle.r;
t = 0;
rho = 1.021e3;
m = 4/3*pi*rho*particle.r^3;

%if the simulation get to an infinite loop it is stopped after a calculated
%time of 10s
countdown = 10;

```

```

if nargin == 11
    % A velocity field is provided
    v = [v_medium 0];
    Fdep0 = calcValue (startPoint(1), startPoint(2), Fdep0_field{1}, Fdep0_field{2});
else
    v = [v_medium 0];
    fem_pd_x = posteval (v_field_OR_femstruct, 'FdepX0');
    fem_pd_y = posteval (v_field_OR_femstruct, 'FdepY0');
    fdepX0 = griddata (fem_pd_x.p(1,:), fem_pd_x.p(2,:), fem_pd_x.d, startPoint(1), startPoint(2), 'linear');
    fdepY0 = griddata (fem_pd_y.p(1,:), fem_pd_y.p(2,:), fem_pd_y.d, startPoint(1), startPoint(2), 'linear');
    Fdep0 = [fdepX0 fdepY0];
end

trajectory = startPoint;

nextPoint = startPoint;

while (~isnan (v(1)) && countdown >= 0 && nextPoint(1) >= rangeX(1) && nextPoint(1) <= rangeX(2))
    if (nextPoint(2) < rangeY(1) || nextPoint(2) > rangeY(2))
        if (returnOnlyTrajectoriesInsideChannel == 1)
            trajectory = [0 0];
        end
    end

    return
end
%apply U factor
Fdep0 = Fdep0 * U.electrode^2;

t = t + timeStep;
%Inertia force can be neglected
v_ges = (Fdep0*particle.r^3*particle.K)/k1 + v;
nextPoint = nextPoint + (v_ges * timeStep);
trajectory = cat(1, trajectory, nextPoint);

if nargin == 11
    v = [v_medium 0];
    Fdep0 = calcValue (nextPoint(1), nextPoint(2), Fdep0_field{1}, Fdep0_field{2});
else
    v = [v_medium 0];
    fdepX0 = griddata (fem_pd_x.p(1,:), fem_pd_x.p(2,:), fem_pd_x.d, startPoint(1), startPoint(2), 'linear');
    fdepY0 = griddata (fem_pd_y.p(1,:), fem_pd_y.p(2,:), fem_pd_y.d, startPoint(1), startPoint(2), 'linear');
    Fdep0 = [fdepX0 fdepY0];
end

countdown = countdown - timeStep;
end

```

calcValue.m

```

function value = calcValue (x, y, dataArr_x, dataArr_y)

%find surrounding coordinates,
%only dataArr_x has to be checked since all
%dataArr's have the same coordinates
i = 1;
while (i <= length(dataArr_x.x) && dataArr_x.x(i) <= x)
    i = i+1;
end

%due to the precision of floating point calculations it could happen that
%the evaluation dataArr_x.x(i) <= x evaluates to 0 for the second point
%even if the values should be 'equal'.
%
% e.g. the expression -9.9e-5 <= -(200e-6/2-1e-6) evaluates to 0, even it
% should be equal.
%
%See http://www.mathworks.com/support/tech-notes/1100/1108.html
%
%The problem arises when the data calculated by Comsol has NaNs for the
%first x-values, so the index i should at least be 2
if i>2
    i = i-1;
end

j = 1;
while (j <= length(dataArr_x.y) && dataArr_x.y(j) <= y)
    j = j+1;
end

j = j-1;

%the indices for the 'data box' has been found, now check the

```

```

%boundaries
%only dataArr_x has to be checked since all
%dataArr's have the same coordinates
if (i <= 0 || j <= 0 || ...
    i+1 > length(dataArr_x.x) || j+1 > length(dataArr_x.y))
    value = [NaN NaN];
    return;
end

%weights
wx = (x - dataArr_x.x(i)) / (dataArr_x.x(i+1) - dataArr_x.x(i));
wy = (y - dataArr_x.y(j)) / (dataArr_x.y(j+1) - dataArr_x.y(j));

%boundaries are ok, now build the linear mean value approximation

%since the data array is flipped for the x and y coordinates we have to
%flip it here too
dataArr = dataArr_x;

value_x = ((dataArr.data(j,i) *(1-wx) + dataArr.data(j+1,i) *wx) * (1-wy) + ...
    (dataArr.data(j,i+1)*(1-wx) + dataArr.data(j+1,i+1) *wx) * ( wy));

dataArr = dataArr_y;
value_y = ((dataArr.data(j,i) *(1-wx) + dataArr.data(j+1,i) *wx) * (1-wy) + ...
    (dataArr.data(j,i+1)*(1-wx) + dataArr.data(j+1,i+1) *wx) * ( wy));

value = [value_x value_y];

```

plotTrajectoriesForWholeChannel.m

```

function simulationSets = plotTrajectoriesForWholeChannel (simulationSets, testParticles, rangeMinMaxY, v_medium, U_electrode, ...
    eta_medium, timeStep, bChannelLength, channelLengthOrCount)

%Calculate the trajectories for the whole channel for all simulation
%sets and test particles. The outcome is plotted for each geometry in an own figure
simulationSets = calcTrajectoriesForWholeChannel (simulationSets, testParticles, rangeMinMaxY, v_medium, U_electrode, ...
    eta_medium, timeStep, bChannelLength, channelLengthOrCount);

for simSetsIndex = 1:size(simulationSets, 2)
    simulations = simulationSets(simSetsIndex).simulations;

    for index = 1:size(simulations,2)
        figure;
        simulation = simulations(index);
        %The title for the figure
        name = strcat('Design ', num2str(simulation.designNr, '%02g'), ', ', c1=',', num2str(simulation.c1), ', ', ew=',', ...
            num2str(simulation.ew), ', ', U=',', num2str(U_electrode), ', ', v=',', num2str(v_medium));
        set(gcf, 'Name', name);
        legend_strs = [];
        hold all;

        if bChannelLength == 1
            calcCount = ceil (channelLengthOrCount / simulation.c1);
        else
            calcCount = channelLengthOrCount;
        end

        for testParticleIndex = 1:size(testParticles, 2)
            particle = testParticles(testParticleIndex).particle;

            if bChannelLength == 1
                trajIndex = channelLengthOrCount * 1e6;
            else
                trajIndex = channelLengthOrCount;
            end

            trajectory = simulation.testParticles(testParticleIndex).trajectoryForWholeChannel{trajIndex};

            plot (trajectory(:,1), trajectory(:,2), 'LineWidth', 2);
            legend_strs = strvcat(legend_strs, strcat('r=', num2str(particle.r), ', ', K=', num2str(particle.K)));
        end

        set(gca, 'XLim', [-(simulation.c1/2) simulation.c1/2+calcCount*simulation.c1], 'YLim', rangeMinMaxY, 'YGrid', 'On');
        h = legend (legend_strs, 3);
        set(h, 'Interpreter','none')
        grid off;
        hold off;
    end
end
end
end

```

B Device fabrication masks

The following figures show the fabrication masks drawn in AutoCAD 2004 for the short and long devices with a separation channel width of $250\ \mu\text{m}$. The masks for the devices with a separation channel width of $300\ \mu\text{m}$ only differ in the width of the separation channel and the electrode geometries.

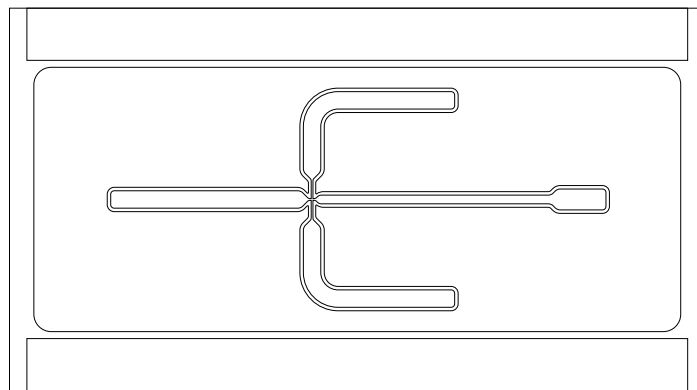


Figure B.1: Mask for the SU8 channel structures on the glass wafer (short device).

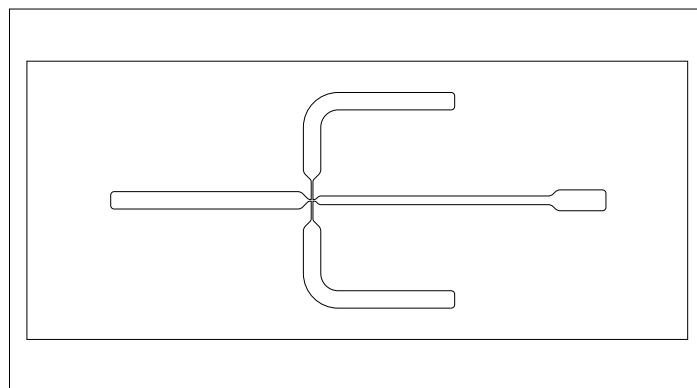


Figure B.2: Mask for the copper layer that protects the SU8 structures that should not be removed from the glass and silicon wafer (short device).

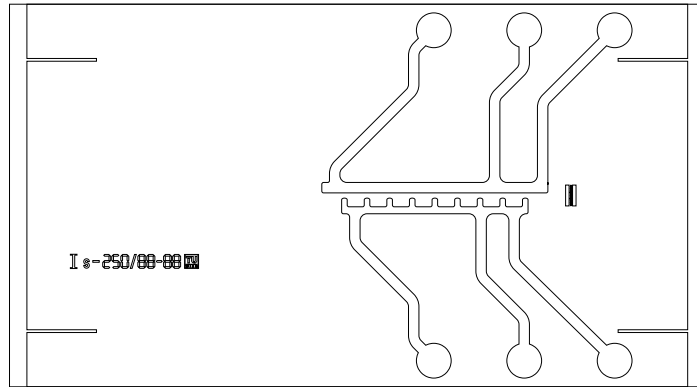


Figure B.3: Mask for the platinum electrodes (short device).

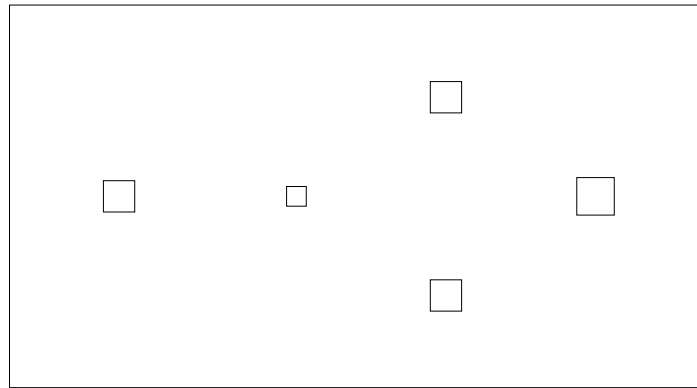


Figure B.4: Mask for the KOH wet etching process (short device).

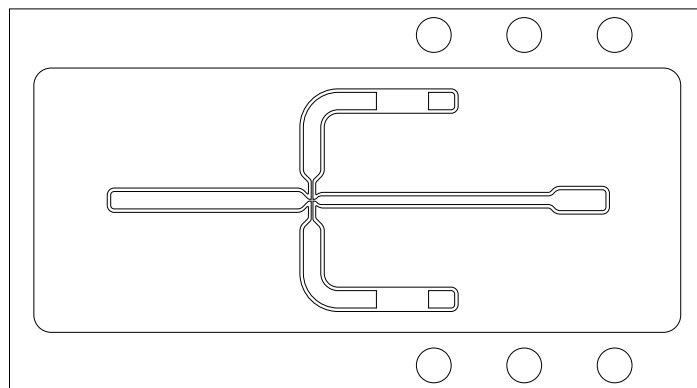


Figure B.5: Mask for the SU8 channel structures on the silicon substrate (short device).

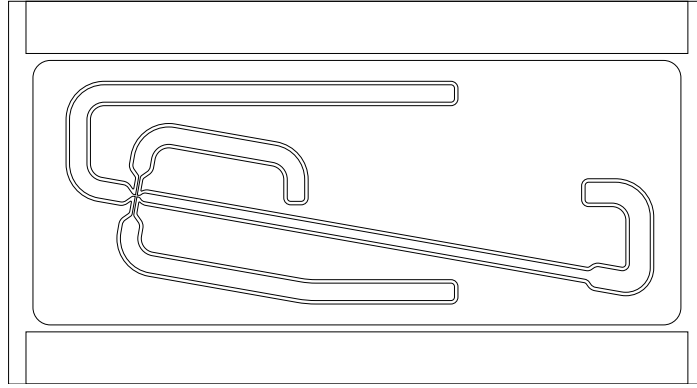


Figure B.6: Mask for the SU8 channel structures on the glass wafer (long device).

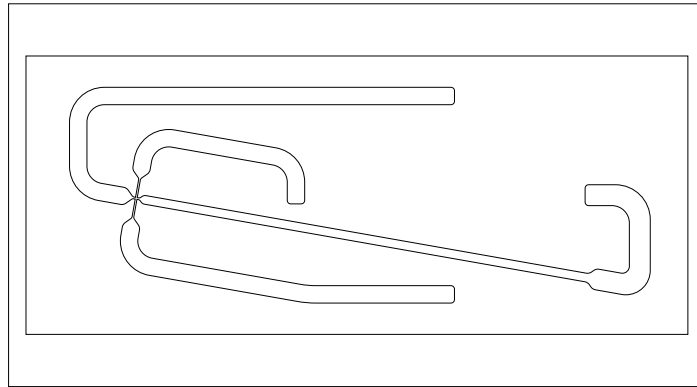


Figure B.7: Mask for the copper layer that protects the SU8 structures that should not be removed from the glass and silicon wafer (long device).

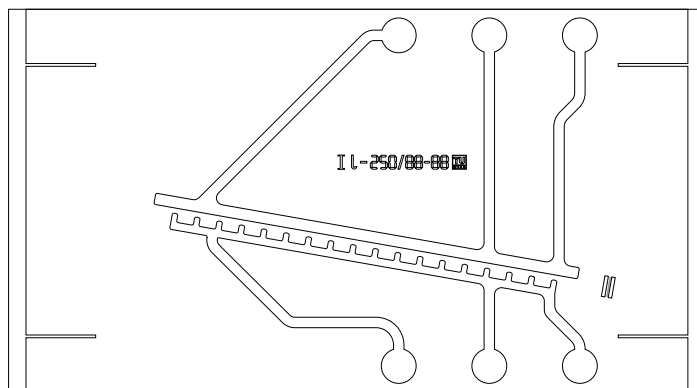


Figure B.8: Mask for the platinum electrodes (long device).

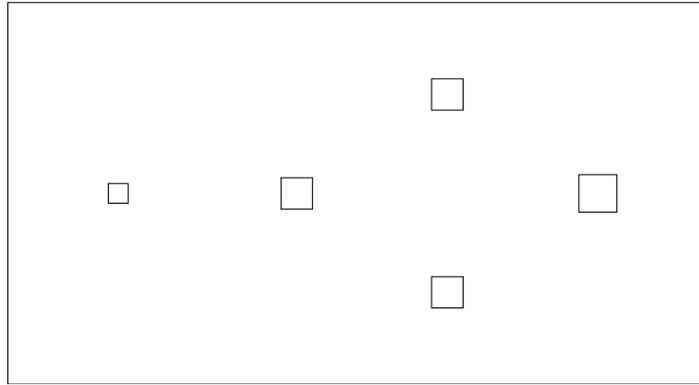


Figure B.9: Mask for the KOH wet etching process (long device).

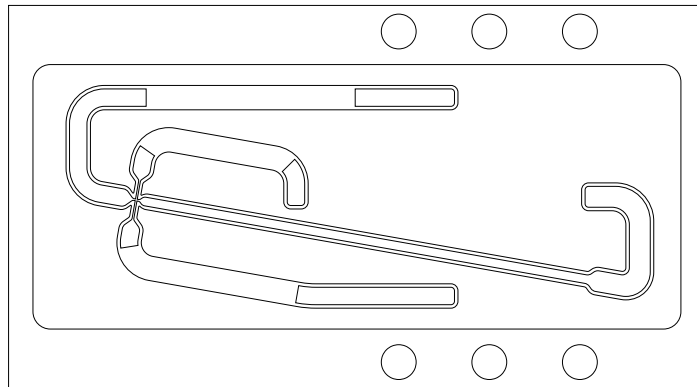


Figure B.10: Mask for the SU8 channel structures on the silicon substrate (long device).

C Measurement work flow

The experience gained during the device measurements are summarized to ease future experimental setups.

First the device has to be fixated on the printed circuit board:

- The device is placed over the aperture in the middle of the PCB. For an easier alignment the copper bars around that aperture are used.
- After the alignment the chip is glued on the PCB with its edges using *Loctite Super Glue*. For this purpose it is sufficient to apply the glue with a brush only at that locations where the device contact the PCB. The glue is drawn between the device and the PCB and the device is fixated after a couple of minutes.

Then the electrodes have to be wire bonded with the pads on the PCB. The following procedure was applied:

- The pads for contacting the device on the PCB are covered with solder.
- A thin copper wire, e.g. an enameled copper wire, is uninsulated and a small eye is formed at one end using a tweezers.
- After shortening the bonding wire to a length of about 7 mm the eye is placed over an electrode contact pad on the device with the tweezers and the wire is soldered onto the pad of the PCB.
- Using a microscope the placement of the eye is improved such that the distance between the wire and the pad is reduced to a minimum.
- Finally the wire is connected to the electrode pad with liquid conductive silver. It consists of small silver particles that are conserved in a solvent that evaporates after the bonding task. The conductive silver can be applied with a thin brush or simply with a toothpick.

After the device is glued onto the PCB and the electrode pads are wire bonded the chip has to be flooded with the desired fluid used for the measurements, e.g. deionized water or mannitol solution:

- After connecting the syringes with the tubes for the sheath and side port inlets of the device holder the tubes are filled with the fluid till the o-rings are covered with the fluid. There should be no air bubbles neither in the syringes nor in the tubes.

- Then the PCB with the device is screwed onto the device holder. An efficient method is to press the device gently onto the the o-rings and fixate the PCB with the screws. It is important to tighten the screws not too firmly. If the screw does not 'turn on its own' anymore the device should be fixated sufficiently.
- The glass cover of the device can be cleaned with ethanol using a cotton bud.
- Then the syringe pumps can be started and the device is flooded at higher flow rates of about 30 μm till all air is removed from the device. Additionally it is a good idea to keep the outlet shut so that fluid leaves the device through the sample inlet, too.

Then the device is removed from the device holder and the following preparations for the measurement process have to take place:

- To prevent the device from running dry the inlets and the outlet on its bottom should be covered with small drops of the fluid. It is important to avoid even the smallest air bubbles.
- The tube for the sample flow is filled with liquid, the device holder is cleaned once again by washing it with deionized water and removing all remaining strands.
- Then the o-rings of the sheath, sample and side port inlets are covered with the fluid by operating the syringe pumps in fast forward mode.
- The device is mounted on the device holder using the technique described above.
- Finally the contact pins on the PCB are connected to the voltage supply.

Now the syringe pumps can be turned on with the desired flow rates.

The following tips may be of additional help:

- For the small flow rates that are needed for the function of the device it is better not to use particle filters for the sheath and side port flows because the filters decrease the responsiveness of the flow rates in the device channels with their damping character.
- Even the smallest air bubbles have to be avoided, especially in the inlets of the device, otherwise the flow rate would fluctuate in the device channel due to the rare syringe pump steps and the compressibility of the bubbles. That can lead to a decreased quality of the particle focusing.
- The parts of the device edges where the electrode pads are placed should not be glued to the PCB to minimize the risk of insulating them by covering the pads with the liquid glue.
- When inlets at the back of the device are covered with small drops of the fluid to avoid drying it is useful to cover the sample inlet with a small drop of sample liquid so that the sample is not thinned too much after mounting the device to the holder.

D μ TAS 2007 conference abstract

ON-CHIP CONTINUOUS CELL SEPARATOR USING POSITIVE AND NEGATIVE DIELECTROPHORESIS

J. Avian, S. Kostner, M.J. Vellekoop

Institute of Sensor and Actuator Systems (ISAS), Vienna University of Technology
Gusshausstrasse 27-29, A-1040 Vienna, Austria, email: avian@isas.tuwien.ac.at

Introduction

In this paper we present a novel design for a continuous separation device for particles and cells based on dielectrophoresis (DEP). Compared to other DEP separators, which rely on negative dielectrophoretic particle behavior [1] or particle traps [2], the separator presented in this contribution works continuously with negative as well as positive DEP forces without trapping the particles at the electrode edges. This is effective for direct sorting of particles or cells and prevents them sticking to electrodes or channel wall.

Theory

The dielectrophoretic force moves polarizable particles in an inhomogeneous electric field according to

$$F_{DEP} = 2\pi\epsilon_m R^3 \cdot \text{Re}[\underline{K}] \cdot \nabla E_0^2 \quad \text{with} \quad \underline{K} = \frac{\epsilon_p - \epsilon_m}{\epsilon_p + 2\epsilon_m}, \quad \text{Re}[\underline{K}] \in [-0.5..1], \quad \epsilon_x = \epsilon_x - j \frac{\sigma_x}{2\pi f}.$$

The Clausius Mossotti factor K depends on permittivity and conductivity of the medium (ϵ_m, σ_m), the particle (ϵ_p, σ_p), and the frequency f . R is the particle radius and E_0 is the electric field.

Separation process

The basic idea of the separation process is outlined in Figure 1. The particles are hydrodynamically focused and then separated along a microfluidic channel with electrodes on each side of the channel. To prevent the particles from being trapped at the electrodes the separation process has to take place in a certain distance from the maxima of the field gradient at the metal surface. In the actual separation zone the isosurface planes for the electric potential are vertically orientated and the dielectrophoretic force is independent of the vertical position of the particles (Fig. 2). Therefore it is sufficient to realize the electrodes as plane electrodes on the bottom of the channel. The small electrodes opposite to the straight electrode cause the inhomogeneity of the electric field. The geometry of those electrodes provides a uniform current density distribution in the metal to minimize erosion. The optimal electrode dimensions were found by simulating the particle displacement along the channel for varying size (ew) and spacing (ul) of these electrodes. The maximum particle deviation denotes the best ratio of those parameters (Fig. 3). The channel is dimensioned for particles of $5\mu\text{m}$ diameter that is about 10% of the maximum displacement in either direction, if the particle starts in the center of the $100\mu\text{m}$ wide separation zone. The area within $50\mu\text{m}$ from the electrodes should not be entered by the particles (forbidden zone), otherwise they might be trapped. Additionally, the potential surfaces are not vertical orientated outside the separation zone as mentioned before. Figure 4 shows the trajectories for two cell types with a different diameter and Clausius Mossotti factor and the expected final position after the separation process. As a result of the distance of the particles to the electrode edges, the trajectories are almost parallel for deviant horizontal starting positions.

Device

The channel boundaries of the device are defined by silicon substrate, glass and SU8 for the bottom, top and side walls, respectively. The channel height is $30\mu\text{m}$. The photomasks used to fabricate the device are shown in Figure 5. Currently the device is being fabricated. Measurements to confirm the operation of the device will be conducted in the coming weeks.

Word Count: 492

REFERENCES

1. "Separation of erythrocytes and latex beads by dielectrophoretic levitation and hyperlayer field-flow fractionation," J. Rousselet, G. H. Markx, R. Pethig, *Colloids and Surfaces (A)*, **140**, 209 (1998).
2. "A Dielectrophoretic Filter for Separation and Collection of Fine Particles Suspended in Liquid," G. Zhou, M. Imamura, J. Suehiro, and M. Hara, *Industry Applications Conference, 2002. 37th IAS Annual Meeting. Conference Record of the*, **2**, 1404 (2002).

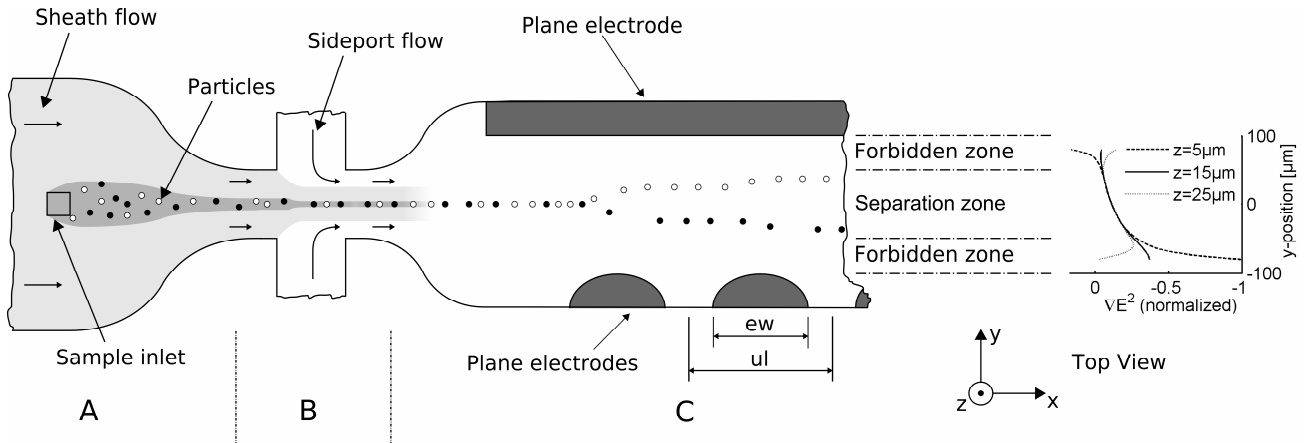


Figure 1: Schematic function of separation process: (A) Particles or cells are injected through the sample inlet etched into the bottom of the device. The sheath flow moves the sample to the taper where the particles are pre-focused horizontally. (B) The second focusing via the sideport flow aligns the particles in a confined row so that all of them enter the separation zone at the same horizontal position. (C) The aligned particles are separated due to their differing size and electrical properties that cause a different dielectrophoretic (DEP) force acting on them. The DEP force is produced by plane electrodes placed at the bottom of the channel.

The diagram on the right shows the normalized DEP force over the y -position in the channel. The separation zone was chosen such that the particles are not exposed to areas where the DEP force shows extreme values and the chance of trapping is high. Depending on the Clausius Mossotti factor the particles are either moved towards the round electrodes (black particles, positive DEP) or away from them (white particles, negative DEP).

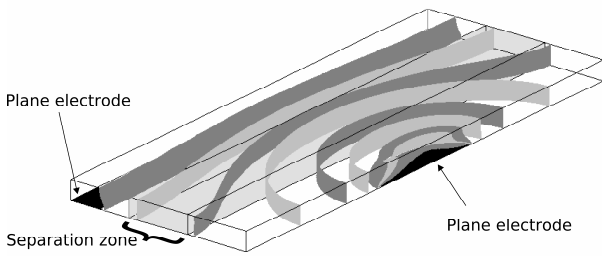


Figure 2: Isosurface planes (gray, dark-gray) of the electric potential for one DEP unit. In the separation zone (light-gray) the surfaces are oriented vertically, in contrast to the planes near the electrodes. Thus the electric field gradient that is responsible for the DEP force is constant for particles at different height.

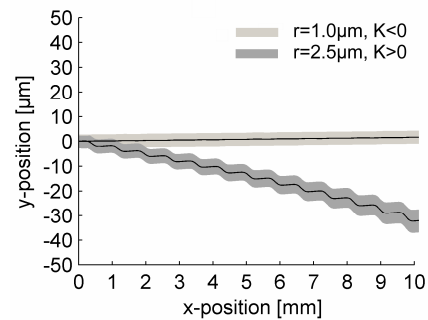


Figure 4: Particle trajectories within the separation zone in a separation channel of 10 mm length for two particles with different size and Clausius Mossotti factor. The electrode voltage V_{rms} is 8V and the particle velocity v_p is 1mm/s. The gray area denotes the trajectory range caused by uncertainties in starting position (injection).

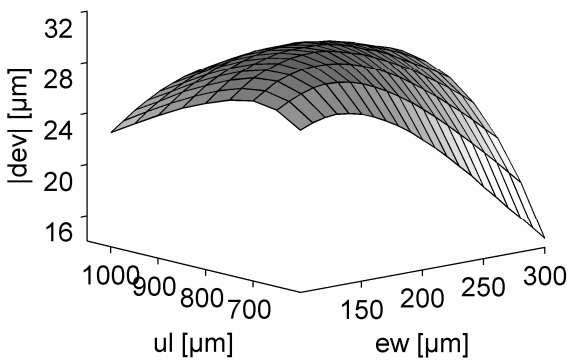


Figure 3: Geometry optimization for the electrodes. The parameters are: electrode width (ew) and DEP unit length (ul), see Fig. 1. The maximum absolute deviation ($|dev|$) corresponds to the lower trajectory in Fig. 4.

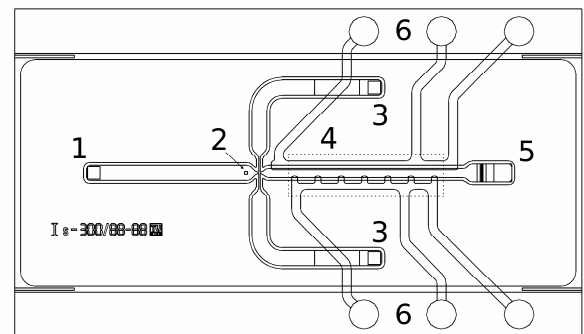


Figure 5: Masks for device fabrication ($11 \times 19 \text{mm}^2$). 1: sheath inlet, 2: sample inlet, 3: side inlets, 4: separation region, 5: outlet, 6: bond pads for electric contacts.

Bibliography

- [Dirschmid, 1992] Dirschmid, H. J. (1992). *Mathematische Grundlagen der Elektrotechnik*. Vieweg Verlagsgesellschaft.
- [Fatoyinbo et al., 2005] Fatoyinbo, H. O., Kamchis, D., Whattingham, R., Ogin, S. L., and Hughes, M. P. (2005). A high-throughput 3-d composite dielectrophoretic separator. *IEEE Transactions on Biomedical Engineering*, 52(7):1347–1349.
- [Fritsche, 1999] Fritsche, W. (1999). *Mikrobiologie*. Spektrum Akademischer Verlag GmbH Heidelberg, Berlin.
- [Hang et al., 2005] Hang, H., Yun, H., Cho, K. C., Chung, C., Han, D.-C., and Chang, J. K. (2005). Expansion channel for microchip flowcytometer. In *9th International Conference on Miniaturized Systems for Chemistry and Life Sciences*, pages 103–105, Boston, Massachusetts, USA.
- [Hölzel, 1997] Hölzel, R. (1997). Electrorotation of single yeast cells at frequencies between 100hz and 1.6 ghz. *Biophysical Journal*, 73:1103–1109.
- [Hölzel, 1999] Hölzel, R. (1999). Non-invasive determination of bacterial single cell properties by electrorotation. *Biochim. Biophys. Acta*, 1450(1):53–60.
- [Hölzel, 2002] Hölzel, R. (2002). Single particle characterization and manipulation by opposite field dielectrophoresis. *Journal of Electrostatics*, 56:435–447.
- [Jones, 1995] Jones, T. B. (1995). *Electromechanics of Particles*. Press Syndicate of the University of Cambridge.
- [Kostner, 2004] Kostner, S. (2004). *On-chip particle separator based on dielectrophoresis*. Institute of Sensor and Actuator Systems, Vienna University of Technology.
- [Li and Kaler, 2002] Li, Y. and Kaler, V. I. S. (2002). Dep based cell separation utilizing planar microelectrode array. In *2002 Annual Report Conference on Electrical Insulation and Dielectric Phenomena*, pages 680–684.
- [Nieuwenhuis, 2005] Nieuwenhuis, J. H. (2005). *Microsystems for particle analysis*. Institute of Sensor and Actuator Systems.
- [Suehiro et al., 2001] Suehiro, J., Noutomi, D., Hamada, R., and Hara, M. (2001). Selective detection of bacteria using dielectrophoretic impedance measurement method combined with antigen-antibody reaction. In *Industry Applications Conference, 2001. Thirty-Sixth IAS Annual Meeting. Conference Record of the 2001 IEEE*, volume 3, pages 1950–1955.

- [Suzuki et al., 2005] Suzuki, M., Yasukawa, T., Shiku, H., and Matsue, T. (2005). Separation of live and dead microorganisms in a micro-fluidic device by dielectrophoresis. *The Japan Society for Analytical Chemistry*, 54(12):1189–1195.
- [Svasek et al., 2003] Svasek, P., Svasek, E., Lendl, B., and Vellekoop, M. (2003). Fabrication of miniaturized fluidic devices using su-8 based lithography and low temperature wafer bonding. In *Sensors and Actuators A*, volume 115, pages 591–599.
- [Zhou et al., 2002] Zhou, G., Imamura, M., Suehiro, J., and Hara, M. (2002). A dielectrophoretic filter for separation and collection of fine particles suspended in liquid. In *IEEE Industry Applications Conference, 2002. 37th IAS Annual Meeting. Conference Record of the*, volume 2, pages 1404–1411.